HHS Public Access

Author manuscript

Sci Transl Med. Author manuscript; available in PMC 2017 November 17.

Published in final edited form as:

Sci Transl Med. 2017 May 17; 9(390): . doi:10.1126/scitranslmed.aal4069.

The effects of micronutrient deficiencies on bacterial species from the human gut microbiota

Matthew C. Hibberd[1,2], **Meng Wu**[1], **Dmitry A. Rodionov**[3,4], **Xiaoqing Li**[4], **Jiye Cheng**[1,2], **Nicholas W. Griffin**[1,2], **Michael J. Barratt**[1,2], **Richard J. Giannone**[5], **Robert L. Hettich**[5], **Andrei L. Osterman**[4], and **Jeffrey I. Gordon**[1,2,*]

[1]Center for Genome Sciences and Systems Biology, Washington University School of Medicine, St. Louis, MO 63110 USA

[2]Center for Gut Microbiome and Nutrition Research, Washington University School of Medicine, St. Louis, MO 63110 USA

[3]A. A. Kharkevich Institute for Information Transmission Problems, Russian Academy of Sciences, Moscow 127994, Russia

[4]Sanford Burnham Prebys Medical Discovery Institute, La Jolla, 92037 CA USA

[5]Chemical Sciences Division, Oak Ridge National Laboratory, Oak Ridge, TN 37830, USA

Abstract

Vitamin and mineral (micronutrient) deficiencies afflict two billion people. While the impact of these imbalances on host biology has been studied extensively, much less is known about their effects on the gut microbiota of developing or adult humans. Therefore, we established a community of cultured, sequenced human gut-derived bacterial species in gnotobiotic mice and fed the animals a defined micronutrient-sufficient diet, followed by a derivative diet devoid of vitamin A, folate, iron or zinc, followed by return to the sufficient diet. Acute vitamin A deficiency had the largest effect on bacterial community structure and meta-transcriptome, with *Bacteroides vulgatus*, a prominent responder, increasing its abundance in the absence of vitamin A. Applying retinol selection to a library of 30,300 *B. vulgatus* transposon mutants revealed that disruption of *acrR* abrogated retinol sensitivity. Genetic complementation studies, microbial RNA-Seq, and transcription factor binding assays disclosed that AcrR is a repressor of an adjacent AcrAB-TolC efflux system. Retinol efflux measurements in wildtype and *acrR*-mutant strains plus

*Correspondence to: jgordon@wustl.edu.

Author Contributions:

M.C.H., A.O., and J.I.G. designed the experiments. Experiments were performed by M.C.H. (generation of gnotobiotic mouse model; COPRO-Seq and microbial RNA-Seq analyses of microbial communities harvested from these mice; growth, INSeq, mass spectrometry and pharmacologic studies of *B. vulgatus* and *B. dorei in vitro*), M.W. (construction of *B. vulgatus* INSeq library), D.A.R. and X.L. (expression and purification of *B. vulgatus* and *B. dorei* AcrR expressed in *E. coli*; *in vitro* assays of AcrR binding to target DNA), R.J.G. (mass spectrometry-based proteomic studies), and J.C. (targeted mass spectrometry of retinol in efflux assays). M.C.H., M.W., D.A.R., N.W.G., R.J.G., R.L.H., A.O., and J.I.G. analyzed the data. M.C.H., M.J.B, A.O., and J.I.G. wrote the paper.

Competing Interests: J.I.G. is co-founder of Matatu, Inc., a company characterizing the role of diet-by-microbiota interactions in animal health. The other authors declare no competing interests.

Data and materials availability: COPRO-Seq, microbial RNA-Seq, and INSeq datasets have been deposited in the European Nucleotide Archive (Accession Number PRJEB15673). All of the bacterial strains used in this work were purchased from American Type Culture Collection (ATCC) or Deutsche Sammlung von Mikroorganismen und Zellkulturen GmbH (DSMZ).

treatment with a pharmacologic inhibitor of the efflux system, revealed that AcrAB-TolC is a determinant of retinol and bile acid sensitivity in *B. vulgatus*. Acute vitamin A deficiency was associated with altered bile acid metabolism *in vivo*, raising the possibility that retinol, bile acid metabolites, and AcrAB-TolC interact to influence the fitness of *B. vulgatus* and perhaps other microbiota members. This type of preclinical model can help to develop mechanistic insights about and more effective treatment strategies for micronutrient deficiencies.

Introduction

Dietary micronutrients (vitamins and minerals) are cofactors for myriad enzymes whose functions are essential for health. The “hidden hunger” of micronutrient deficiencies represents a global health challenge, affecting 2 billion individuals, with deficiencies in iron, zinc, folate and vitamin A representing major contributors to this problem (1, 2). Risk is compounded in low and middle income countries where dietary insufficiency and lack of dietary diversity are common (3).

Vitamin A plays important roles in vision, growth, and immune function (4). In settings where its deficiency is a public health problem, the World Health Organization (WHO) recommends high-dose vitamin A supplementation for infants and children 6–59 months of age (5). Vitamin A is typically given in the form of retinyl esters, which are hydrolyzed in the gut prior to uptake of retinol by enterocytes (6). The effectiveness of vitamin A supplementation has been confirmed in a meta-analysis of 43 studies showing a reduction in mortality in children under 5 (7). However, knowledge of the short and long term effects of high dose supplementation of infants and children is incomplete. Given the large body of knowledge that has accumulated regarding the effects of retinoids on eukaryotic cellular biology, vitamin A imbalances are typically viewed from the perspective of their effects on the host, rather than on the microbiota.

Deficiencies of other micronutrients are also associated with morbidity in children under 5 (1). Given the prevalence of multi-deficiencies in individuals living in low and middle income countries, many studies have been conducted to examine the benefits of multiple micronutrient powders. A meta-analysis of 16 controlled studies of supplementation with micronutrient powders in 6-month to 11-year old children revealed a reduction in anemia and improved serum hemoglobin levels, but no impact on growth (8). There was also evidence of increased diarrhea (9). Studies of weaning Kenyan infants revealed evidence of increased intestinal inflammation, increased enteropathogen burden, and decreases in the representation of bifidobacteria associated with administration of micronutrient powders containing iron (10). Moreover, iron supplementation may potentiate the risk for certain systemic infections (e.g., malaria) (11–14). Together, these findings raise questions about whether current protocols for dosing and duration of treatment of micronutrient deficiencies are optimal, and to what extent unintended deleterious effects accompany such interventions.

Recent studies have revealed a program of gut microbial community development, defined by changing patterns of abundance of a group of age-discriminatory bacterial strains, that is executed during the first 2–3 years of postnatal life (15–17). This developmental program is shared among healthy, biologically-unrelated infants and children living in culturally and

geographically distinct low income countries; and it is disrupted in infants and children with undernutrition, resulting in bacterial community configurations that appear younger (more immature) compared to those encountered in chronologically age-matched individuals with healthy growth phenotypes (14, 16, 18). Preclinical evidence indicates that this immaturity is not simply an effect of undernutrition but rather is a contributing cause. Recently weaned gnotobiotic mice colonized with immature gut microbiota samples from undernourished Malawian children exhibited impaired growth compared to recipients of microbiota from chronologically age-matched healthy donors, even though animals in all treatment groups consumed the same amounts of a macro- and micronutrient deficient diet designed to resemble the diets of the microbiota donor population. Analysis of the gut microbial communities of recipient mice identified bacterial strains that are growth-discriminatory: they include a subset of the age-discriminatory strains (16). These observations suggest a testable hypothesis, namely, that various types of micronutrient imbalances may disrupt various features of a developing microbiota, including the representation and expressed functions of age- and growth-discriminatory taxa as well as pathobionts and enteropathogens. Moreover, such disruptions, occurring during a critical period of community assembly, may persist, resulting in deleterious effects on host biology. A corollary is that the microbiota may be a useful marker of micronutrient intake (19), and a means to assess the efficacy and safety of current dosing regimens for treatment of deficient states.

Earlier studies comparing germ-free animals and their conventionally-raised counterparts provided evidence that the gut microbiota can have beneficial effects in the face of micronutrient deficiencies (e.g., enhanced iron uptake and storage in rats and rabbit models; 20, 21), or detrimental effects [increased mortality on vitamin A-deficient diets (22, 23), and increased dietary zinc requirements (21, 24) in rats]. The specific microbes and underlying mechanisms responsible for these observed effects were not defined in these reports.

There is little information about the effects of specific micronutrient imbalances on the human gut microbiota (10, 19, 25–28). The limited number of published reports have been descriptive, focused on community structure (generally at low levels of taxonomic resolution), and are confounded by (i) the challenges of conducting randomized controlled trials in this area, (ii) the fact that various combinations of micronutrient deficiencies can occur within at risk populations, and (iii) the challenge of distinguishing between primary effects of dietary micronutrient content, versus host effects, on the microbiota. In the current study, we examine the effects of acute dietary micronutrient deficiencies on members of the microbiota using gnotobiotic mice colonized with a large and phylogenetically diverse consortium of cultured and sequenced human gut bacterial strains, including strains representing species that are age-and/or growth-discriminatory in models of microbiota development (14, 16, 17). Mice were subjected to a diet oscillation that began with a defined micronutrient-sufficient diet followed by a derived diet with one of four types of single micronutrient deficiency, or a diet representing combined deficiencies, followed by return to the original micronutrient-sufficient diet. This model of acute deficiency allowed us to focus on effects on the gut microbiota, rather than having to disentangle potentially cofounding effects of combined community and host deficiency states. Bacterial community DNA and mRNA analyses, combined with *in vitro* genetic, biochemical and pharmacologic studies

allowed us to characterize the mechanisms that underlie the pronounced effects of vitamin A, specifically retinol, deficiency on the fitness of *Bacteroides vulgatus*, a growth-discriminatory species identified in the gnotobiotic mouse model of human gut microbiota development described above. Our findings provide a rationale and a preclinical method for examining the impact of current vitamin A dosing regimens, and by extension other critical micronutrients, on members of our microbial communities, including the developing gut microbiota of children with undernutrition.

Results

A compositionally well-defined, micronutrient-sufficient diet, and a set of highly similar derivative diets devoid of one or more micronutrients, were designed (table S1). Protein was represented in all diets only by amino acids; this feature allowed us to avoid the potentially confounding problem of having to vary protein type due to differences in their content of bound minerals. Adult (8–9 week old) germ-free C57Bl/6J mice that had been weaned onto a standard mouse chow, rich in plant polysaccharides and low in fat, were placed on the micronutrient-sufficient diet for four days prior to colonization. Animals then received a single oral gavage of a consortium of 92 sequenced human gut-derived bacterial type strains, containing 348,834 known or predicted protein-coding genes, and encompassing the major phyla present in the human microbiota. Sixteen of these strains represented species corresponding to strains that had been identified as age- and/or growth-discriminatory in Random Forests-derived models of normal gut microbiota development (table S2). Mice in each experimental group were maintained on the micronutrient-sufficient diet for 14 days, followed by a 21-day period of acute micronutrient deficiency (one of five diets: vitamin A-deficient; folate-deficient, iron-deficient, zinc-deficient and multiple micronutrient-deficient), followed by a 14-day period of re-exposure to the micronutrient-sufficient diet. A control group was maintained on the micronutrient-sufficient diet throughout the course of the experiment (Fig. 1A). All diets were provided *ad libitum*.

Short-read shotgun sequencing (COmmunity PROfiling by Sequencing; COPRO-Seq) of DNA prepared from fecal samples collected over time was used to define the efficiency and reproducibility of colonization within and across treatment groups, and the relative abundance of each community member as a function of diet. A group of 44 strains comprised a core group of organisms that was represented in the fecal microbiota of all mice after the initial micronutrient-sufficient diet phase; the number of additional strains found in each treatment group was small (range 0–3) (table S3A,B). This similarity in community membership across treatment groups at the end of this stage of the experiment was reflected in principal coordinates analysis (PCoA) of pairwise comparisons using the Bray-Curtis dissimilarity metric (Fig. 1B, fig. S1). We cannot rule out the possibility that other members of the consortium of 92 organisms established themselves in different regions of the gut, even though they were not detectable in feces. Investigating this possibility would require sacrifice of multiple animals at multiple time points in each of the multiple treatment groups to perform a detailed analysis of the biogeographical features of their microbial communities.

Acute dietary vitamin A deficiency has the greatest effect on community structure and meta-transcriptome

We applied mixed-effects linear models to log-transformed, rarefied COPRO-Seq data to identify organisms with significant interactions between treatment group and diet stage. We also performed least-squares means comparisons between mice in the control group monotonously fed the micronutrient-sufficient diet and those assigned to the experimental treatments (table S4A,B). Communities sampled at the end of the initial micronutrient-sufficient diet phase (experimental day 14), 14 days after switch to the deficient diet (day 28) and 14 days after return to the sufficient diet (day 49) were included in the analyses. The results revealed that among the five acute dietary deficiency states tested, vitamin A had the greatest effect, significantly impacting the abundances of the largest number of organisms (table S3A–G, table S5A–C). Comparisons of Bray-Curtis dissimilarities showed that the community structure of mice in the vitamin A treatment group differed significantly from that of the control group during the deficient diet stage [experimental days 28 and 35; $P<0.01$ for each experimental day based on randomization tests and False Discovery Rate (FDR) correction, but was no longer significantly different after returning to the sufficient diet (experimental day 49)] (fig. S1). The number of species representing age- and growth-discriminatory strains that were affected by acute micronutrient deficiency was small (range 0–3/deficiency type; see table S4A for details and table S4B for a summary).

We subsequently used microbial RNA-Seq to characterize transcriptional responses to the various diets. Data generated from fecal samples collected from each mouse in each treatment group at the end of the micronutrient sufficiency phase (day 14), the end of the micronutrient deficiency phase (day 35), and 14 days after return to the sufficient diet (day 49) were compared. Statistically significant differences in gene expression as a function of time/diet were identified (see Materials and Methods). Responsive genes were binned into KEGG Orthology (KO) groups. Analogous to the COPRO-Seq analysis, animals consuming the micronutrient-sufficient diet monotonously served as a reference control for temporal effects independent of diet transitions.

table S6A–H describes the results of this community-wide (top-down) RNA-Seq analysis for all treatment groups. Vitamin A deficiency elicited a larger number of significant alterations in the meta-transcriptome than any of the other acute deficiency states (summarized in table S6A with KEGG summaries of differentially expressed genes and associated *P*-values provided in table S6B). The two top ranked KEGG Orthology groups that incorporated transcripts whose expression changed significantly as a function of the presence and absence of vitamin A were K02014 (TonB dependent receptors), and K00936 (phosphotransferases with a nitrogenous group as acceptor) (table S6B).

B. vulgatus, a species positively correlated with host growth in preclinical models of gut microbiota development (16), was one of the few age- and/or growth-discriminatory taxa that exhibited significant changes in abundance as a function of any of the acute dietary micronutrient deficiencies applied; its proportional representation in the community increased significantly during the vitamin A deficiency phase and decreased significantly when mice were transitioned back to the sufficient diet (Fig. 1C, fig. S2A; $P<0.001$, one-way ANOVA, Tukey's HSD test, FDR correction). Mixed effects linear modeling revealed that

no other single micronutrient deficiency produced a statistically significant increase in the representation of *B. vulgatus* (table S4). The only other single micronutrient deficiency state that affected its representation was iron deficiency, but the change occurred in a direction opposite to that observed with vitamin A deficiency (Fig. 1C, fig. S2A, table S4). The direction and specificity of the response to vitamin A deficiency was notable, as none of the other *Bacteroides* in the community exhibited this pattern (table S5).

The microbial RNA-Seq dataset revealed the specificity and distinctive breadth of responses of *B. vulgatus* to vitamin A availability (see table S7A–G for a KEGG Orthology group-level summary of significant changes in its *in vivo* gene expression profile in response to diet oscillations involving vitamin A, iron, zinc, or folate, and combined deficiency, as well as in the control group monotonously fed the micronutrient sufficient diet; see table S8A–T for a KEGG Orthology group-level summary of transcriptional responses for each member of the gut microbial community defined as responsive to dietary vitamin A manipulation based on changes in their relative abundance). None of the micronutrient-deficient diets resulted in a significant change in body weight in these adult mice (table S9; $P>0.05$, two-way, repeated measures ANOVA, Dunnett's test).

Identification of a member of the TetR family of transcriptional repressors that mediates the sensitivity of *B. vulgatus* to retinol

To examine the mechanisms underlying the *in vivo* response of *B. vulgatus* to dietary vitamin A availability, we cultured the strain *in vitro*, under anaerobic conditions, in a defined medium, with or without addition of a range of concentrations of retinol, retinal, retinyl palmitate, all-trans retinoic acid or β-carotene; the diterpene alcohol geranylgeraniol was used as a control. Retinoid sensitivity was defined as the ratio between the time required to reach an OD_{600} threshold of 0.3 for treated cultures versus control cultures containing vehicle alone (0.02% DMSO). The concentration range (0.1–10 μM) of retinol and other retinoids used was based on previous reports of their concentrations in mouse small intestinal contents and feces and human feces (29, 30). Treatment with 10 μM retinol completely inhibited the growth of *B. vulgatus* [$P<0.0001$, compared to control incubations containing vehicle (0.02% DMSO) alone]; retinal ($P<0.0001$) and retinyl palmitate ($P=0.0002$) also produced significant, though much weaker, growth inhibition compared to retinol at the same concentration; in contrast, geranylgeraniol had no significant effect ($P>0.99$, one-way ANOVA, Bonferroni multiple comparisons test; Fig. 2A,B, table S10A). A primary isolate of *B. vulgatus* recovered from a Malawian child, characterized as a growth-discriminatory strain in prior gnotobiotic mouse experiments (16), also exhibited marked, dose-dependent growth suppression in the presence of retinol (Fig. 2C, table S10B).

The COPRO-Seq dataset revealed that *Bacteroides dorei* strain DSM-17855 exhibited a response to vitamin A deficiency that was the opposite of that manifested by *B. vulgatus*; namely, it increased rather than decreased its relative abundance in the presence of vitamin A (Fig. 1C, fig. S2B, table S5). Consistent with the responses documented *in vivo* (Fig. 1C, fig. S2B), retinol produced significantly less growth inhibition of *B. dorei in vitro* compared to *B. vulgatus* ($P<0.0001$ for both 5 μM and 10 μM retinol compared to vehicle alone control incubations, t-test, Bonferroni correction; Fig. 2B, table S10A).

Whole genome transposon mutagenesis (INsertion Sequencing, INSeq; 31, 32) was subsequently used to identify the genetic determinants of the response of *B. vulgatus* ATCC 8482 to retinol. A library of 30,300 isogenic transposon (Tn) mutants was generated (see Materials and Methods). 71% (2894) of the strain's predicted genes contained Tn mutants positioned within the first 80% of each open reading frame (ORF) (average of 10.5 Tn mutants/ORF represented in the library; 1 Tn insertion per mutant bacterial strain) (fig. S3A). Simulating the number of unique mutants required to cover all non-essential ORFs (defined as genes that are not required for survival in the medium used to generate the library) (32) revealed that the INSeq library approached saturation (fig. S3B).

The library of Tn mutants was subjected to *in vitro* selection in the presence of 10 μM retinol. Aliquots were withdrawn from primary cultures during the long lag phase (indicating that growth of most members of the library was severely inhibited by retinol) and during stationary phase. An aliquot from the stationary phase culture was then re-inoculated into fresh medium containing 10 μM retinol for a second round of selection; log and stationary phase samples were withdrawn from these secondary cultures (n=3 replicate primary and secondary cultures; Fig. 3A). The selected *B. vulgatus* libraries contained only four mutants (Fig. 3B). These mutants map to two adjacent genes in the *B. vulgatus* ATCC 8482 genome; *BVU0240*, encoding a homolog of *E. coli* AcrR (17% identity, 22% similarity), a member of the TetR family of transcription factors, and *BVU0241*, which encodes a homolog of *E. coli* LpxA (33% identity, 35% similarity). LpxA is a UDP-N-acetylglucosamine O-acyltransferase that functions as the first enzyme in the biosynthetic pathway for the lipid A moiety of lipopolysaccharide [transfers (*R*)-2-hydroxymyristate from its acyl carrier protein thioester to the 3'OH of UDP-N-acetylglucosamine (33)]. Control DMSO-treated cultures displayed no selection for these mutants in either the primary or secondary cultures.

As shown in Fig. 3C, the *B. vulgatus acrR* ortholog is positioned in the middle of a locus containing 12 similarly oriented ORFs. Three ORFs located upstream of *acrR* and three ORFs located immediately downstream each encode orthologs of components of the *E. coli* AcrAB-TolC complex. AcrAB-TolC is the prototypic example of broad specificity multidrug efflux systems belonging to the Resistance-Nodulation-Cell Division superfamily (34, 35). The AcrB component of this complex is a homotrimeric integral inner membrane transporter powered by a proton gradient. TolC is also a homotrimer and resides in the outer bacterial membrane. AcrA, a homohexamer, is a periplasmic adapter protein that bridges AcrB and TolC. Substrates are captured in the lower cleft region of AcrB (through a process determined in part by an associated small accessory protein, AcrZ), transported through the binding pocket, the gate, and finally to the AcrA funnel that connects AcrB to TolC (36, 37) (Fig. 3D). Although the transcriptional repressor AcrR is an important modulator of expression of the AcrAB-TolC system, this efflux pump is also subject to additional regulation by other transcription factors, including those involved in mediating responses to cellular stress signals (38, 39).

Monocultures of each mutant strain exhibited a marked decrease in retinol sensitivity compared to the wildtype strain (Fig. 3E; P<0.0001 for 10μM retinol, one-way ANOVA, Bonferroni multiple comparisons test). To confirm that the *B. vulgatus* AcrR ortholog was a

key regulator of the retinol sensitivity phenotype, we used the integrating expression vector pNBU2_tetQ (40) to complement the mutant containing the Tn insertion at genomic location 361472 (138 nucleotides downstream of the start of the AcrR ORF). To do so, the *BVU0240* (AcrR) ORF and the 21 nucleotide intergenic region between *BVU0240* and *BVU0241* were linked to the promoter of *rpoD* (*BVU2738*), assembled into pNBU2_tetQ, and conjugated into the *B. vulgatus acrR_361472::IN* strain (abbreviated *acrR::IN*) (see Materials and Methods and table S11). Insertion occurred at the *attBV* site positioned at the 3' end of *BVU2094* (one of two serine tRNAs in the *B. vulgatus* genome). Complementation of *acrR::IN* with the vector carrying *PrpoD_acrR* (pNBU2_*acrR*) restored retinol sensitivity to that of the wildtype strain, whereas complementation of *acrR::IN* with the empty pNBU2_tetQ vector had no effect on retinol sensitivity (Fig. 3F; table S10C,D; $P>0.05$ and $P=0.01$, respectively, one-way ANOVA, Bonferroni multiple comparisons test).

Characterizing the regulon controlled by AcrR

Having established that *acrR* (*BVU0240*) is a key genetic determinant of retinol sensitivity *in vitro*, we characterized its regulon. Triplicate cultures of the wildtype, *acrR::IN* and *lpxA_362422::IN* (abbreviated *lpxA::IN*) strains were grown to mid-log phase in the absence of retinol. Microbial RNA-Seq revealed that expression of the *lpxA* ortholog (*BVU0241*) was completely ablated by the Tn insertion in its ORF (*lpxA::IN* mutant). Low expression of *acrR* was detectable in the *acrR::IN* mutant but all reads mapped to the area encompassed by the 5' 138 nucleotides of the gene, indicating that only truncated transcripts derived from the region of *BVU0240* upstream of the Tn insertion site at genome coordinate 361472 were produced. Transcription of the 12 gene locus containing *acrR* and *lpxA* was affected in similar ways by Tn mutagenesis of either *acrR* (*BVU0240*) or *lpxA* (*BVU0241*): i.e., expression of upstream genes was significantly increased (and expression of downstream genes significantly decreased, as would be anticipated by polar effects of the upstream Tn insertion) (Fig. 4, table S12B). Together, these results support a conclusion that the AcrR encoded by *BVU0240* acts as a transcriptional repressor.

A total of 220 genes with statistically significant differences in their expression were identified when comparing the isogenic wildtype and *acrR::IN* strains, and 165 genes when comparing wildtype and *lpxA::IN* strains, with 92 genes common to both datasets. The fold-differences in expression of these 92 genes between the wildtype versus *acrR::IN* and the wildtype versus *lpxA::IN* mutants were highly correlated (Pearson's r = 0.92, $P<0.0001$; these differentially-expressed genes are functionally annotated in table S12A,B, which also describes the fold-differences in their expression both in the comparisons of wildtype and *acrR::IN* strains and wildtype and *lpxA::IN* strains). table S12A highlights genes with shared transcriptional responses to insertional mutagenesis of *acrR* or *lpxA in vitro*: a number of these genes are present in clusters (putative operons) distributed throughout the *B. vulgatus* genome, including polysaccharide utilization loci (PULs), capsular polysaccharide biosynthesis (CPS) loci, plus loci involved in carbohydrate, amino acid and DNA metabolism, as well as drug resistance.

Inspection of the RNA-Seq datasets generated from the fecal microbiota of mice subjected to dietary vitamin A deficiency disclosed that only 18 genes in the putative regulon

identified from the *in vitro* analysis satisfied our statistical threshold for significant differential regulation *in vivo*. The log-normalized fold-changes for these genes ranged from −4.9 to 4.6; however, only nine of these genes displayed a transcriptional response in the same direction as that expected based on the *in vitro* data (table S12B). Notably, genes in the AcrAB-TolC locus did not reach the level of statistical significance we required for designation as differentially regulated *in vivo*.

Identification of a candidate AcrR-binding motif

Comparison of the genomes of other *Bacteroides* strains represented in the defined community, other human gut *Bacteroides*, and other members of the family Bacteroidaceae demonstrated that *acrR* orthologs are positioned in loci containing genes encoding components of multidrug efflux systems belonging to the Resistance-Nodulation-Cell Division superfamily (Fig. 5A, table S13). Fig. S4 presents a phylogenetic tree of AcrR orthologs identified in these organisms (note that *B. dorei* has the highest degree of similarity to *B. vulgatus* AcrR encoded by *BVU0240*; table S13B).

We used comparative genomics of *B. vulgatus* ATCC 8482 and related organisms to identify a conserved 30-basepair (bp) palindrome as a candidate AcrR-binding motif (Fig. 5B,C; this motif is located just upstream of *BVU0244*, the first gene in the locus encoding AcrAB-TolC1 and AcrAB-TolC2 shown in Fig. 3C). Genome scans with this motif allowed reconstruction of predicted AcrR regulons, including orthologs of *BVU0244-BVU0233* (table S13A). As noted above, in *B. vulgatus* ATCC 8482 this gene cluster encodes two homologous AcrAB-TolC efflux pumps; however, their respective components only share 20–27% amino acid identity. Interestingly, in *B. thetaiotaomicron* and several other *Bacteroides* genomes, the orthologous AcrR-associated gene cluster is broken into two separate loci, each encoding one paralog of the AcrAB-TolC efflux system and preceded by a candidate AcrR binding site (Fig. 5A, table S13A), suggesting co-regulation by AcrR orthologs in these genomes.

Genomic searches yielded one additional locus in *B. vulgatus* ATCC 8482 (*BVU0421-BVU0415*) that is preceded by a high-scoring candidate AcrR-binding site (Fig. 5B). This additional candidate AcrR target operon contains genes encoding an uncharacterized outer membrane protein (*oma87*), sodium/sulfate symporter (*slt*), 3'-phosphoadenosine 5'-phosphosulfate (*cysQ*), adenylylsulfate kinase (*cysC*), and sulfate adenylyltransferase (*cysDN*). The latter enzymes are involved in the sulfate assimilation pathway. These *B. vulgatus* genes exhibited increases in their *in vitro* expression in *acrR::IN* and *lpxA::IN* strains compared to wildtype strains (i.e., they are part of the regulon controlled by AcrR), but did not manifest differences *in vivo* as a function of dietary vitamin A content (see table S12B which includes *P*-values).

We subsequently used *in vitro* DNA-binding assays to test the predicted AcrR binding site upstream of *BVU0244* and determined whether retinol affects binding of AcrR from *B. vulgatus* ($AcrR_{BV}$) and *B. dorei* ($AcrR_{BD}$, encoded by *BACDOR00223*). The predicted 30 nucleotide (nt) binding site upstream of the orthologous AcrAB-TolC operon in *B. dorei* has a single nucleotide variation located inside the non-conserved center of the AcrR binding motif. $AcrR_{BV}$ and $AcrR_{BD}$ differ by three amino acid substitutions. Two substitutions are

located in the N-terminal DNA-binding domain, whereas a single substitution is positioned inside the effector binding domain. We also noticed that the annotated $AcrR_{BV}$ ORF in *B. vulgatus* is 24-nt shorter than its ortholog in *B. dorei*, which encodes an additional eight amino acid segment at its N-terminus. This N-terminal sequence is conserved in AcrR orthologs across all analyzed *Bacteroides* spp., suggesting its functional relevance and that the site of initiation of translation of the transcript arising from *acrR* in *B. vulgatus* may have been previously mis-annotated. Therefore, we expressed the full length ($AcrR_{BV}$) and truncated ($AcrR^*_{BV}$) versions of AcrR, as well as its *B. dorei* DSM 17855 ortholog ($AcrR_{BD}$), each fused to a Smt3-His6 tag, in *E. coli*. The recombinant proteins were purified, their tag was removed, and their ability to bind the predicted DNA operator upstream of *BVU0244* (*acrA*) was tested by electrophoretic mobility shift assay and by fluorescence polarization assay (Fig. 5D, fig. S5A–C). Fluorescence polarization assays yielded K_d values of 18.5±6 nM and 25.5±11 nM for $AcrR_{BV}$ and $AcrR_{BD}$, respectively (fig. S5B). In contrast, the truncated $AcrR^*_{BV}$ protein did not interact with the same target DNA fragment. Retinol (up to 125 μM) had no effect on the binding of either purified AcrR ortholog to the target DNA in either assay (fig. S5A,B). These findings are consistent with our analysis of the *in vivo* transcriptional responses of *B. vulgatus*: i.e. that components of its AcrAB-TolC efflux pump, as well as the great majority of other genes in its predicted AcrR regulon, did not show significant differences in their expression as a function of the presence or absence of vitamin A in the diet. This conclusion is also supported by the results of a high resolution quantitative mass spectrometry analysis of the wildtype *B. vulgatus* proteome expressed after growth in medium containing a sub-inhibitory concentration of retinol (1 μM) versus vehicle alone (0.02% DMSO; table S14). Finally, these binding assays also suggest that the differential sensitivity of the two *Bacteroides* species cannot be simply ascribed to differences in the interactions of AcrR with either retinol or the identified target DNA binding site.

Further evidence that the bacterial AcrAB-TolC efflux system affects retinol sensitivity

We hypothesized that the AcrAB-TolC efflux system, whose expression was upregulated when expression of the *acrR* repressor was abrogated, operated to reduce local toxic concentrations of retinol in either the periplasm or cytoplasm. To test this hypothesis more directly, we measured the efflux of retinol from cultures of wildtype *B. vulgatus* and the isogenic *acrR::IN* and *PrpoD_acrR* complemented *acrR::IN* mutants. Equal numbers of stationary phase cells were pelleted and resuspended in PBS containing cysteine and 10 μM retinol. Ultra-performance liquid chromatography-mass spectrometry was used to quantitate retinol in cell free supernatants harvested at various time points during a 2h incubation. We found a statistically significant increase in extracellular retinol in the *acrR::IN* mutant where the efflux machinery was transcriptionally upregulated but not in the wildtype or complemented strains (P=0.01, *acrR::IN* vs wildtype, and *acrR::IN* vs complemented strains; two-way, repeated measures ANOVA, Tukey's HSD test; Fig. 6A).

Phenylalanine-arginine β-naphthylamide (PAβN) is a known inhibitor of multidrug efflux systems, including AcrAB-TolC (41). Wildtype, *acrR::IN*, and complemented strains of *B. vulgatus* were treated with PAβN in the presence or absence of retinol; wildtype *B. dorei* was used as a reference control (unlike wildtype *B. vulgatus*, it is resistant to retinol-

mediated growth inhibition; Fig. 2B). Incubation of the *B. vulgatus acrR::IN* strain (which exhibits increased expression of its efflux system components compared to wildtype), or wildtype *B. dorei* with 25 μg/mL PAβN in the absence of retinol did not result in a statistically significant effect on growth compared to untreated control cultures ($P>0.99$, *B. vulgatus acrR::IN*, $P>0.99$ wildtype *B. dorei*; one-way ANOVA, Bonferroni multiple comparisons test; table S15A). However, addition of the efflux pump inhibitor produced a significant increase in retinol sensitivity in the *B. vulgatus acrR::IN* mutant ($P<0.0001$) and in wildtype *B. dorei* ($P<0.0001$) compared to cultures with retinol alone (Fig. 6B, table S15A; one-way ANOVA, Bonferroni multiple comparisons test). Whereas the wildtype and complemented mutant strains of *B. vulgatus* displayed a modest but significant inhibition of growth in the presence of 25 μg/mL PAβN ($P<0.0001$, both strains), their growth was completely inhibited by 10 μM retinol in both the presence and absence of the efflux pump inhibitor (Fig. 6B, table S15A; one-way ANOVA, Bonferroni multiple comparisons test). Together, these results support the notion that the AcrAB-TolC efflux pump mediates resistance to the growth inhibitory effects of retinol. The precise mechanism by which retinol suppresses growth of *B. vulgatus* remains to be defined.

The effects of bile acids on growth of *B. vulgatus*

UPLC-mass spectrometry disclosed differences in the proportional representation of several bile acid species in the fecal microbiota of the vitamin A-deficient and multiple-deficiency gnotobiotic mouse groups compared to the control group monotonously fed the micronutrient-sufficient diet. For example, vitamin A deficiency was associated with a statistically significant increase in tauro-β-muricholic acid sulfate at the end of the micronutrient-deficiency phase at experimental day 35 ($P=0.02$ for both the vitamin A-deficient and multiple micronutrient-deficient groups compared to micronutrient-sufficient controls; two-way ANOVA, Bonferroni multiple comparisons test; table S16). Tauro-β-muricholic acid is a potent antagonist of the farnesoid X receptor (42). Concentrations of this bile acid, and its sulfated form, correlate with slower intestinal transit time (43).

Examination of the community meta-transcriptome revealed that vitamin A deficiency was associated with differential expression of several genes involved in bile acid metabolism, including bile salt hydrolases (EC3.5.1.24 or K01442) from *B. vulgatus* (*BVU2699*, *BVU3993*), *B. dorei* (*BACDOR00823*), and *B. thetaiotaomicron* (*Bthe7330970*). Of the two *B. vulgatus* bile salt hydrolase transcripts, *BVU2699* was identified as a member of the *acrR* regulon (table S12B).

AcrAB-TolC systems have been reported to contribute to bile acid resistance in bacteria (35, 44). Therefore, we tested the *in vitro* sensitivities of the wildtype and *acrR::IN* strains of *B. vulgatus* to six bile acid species (cholic, deoxycholic, glycocholic, taurocholic, β-muricholic and tauro-β-muricholic acids; concentration range 25–1000 μM), in the presence or absence of the pharmacologic inhibitor of the efflux pump. Wildtype *B. vulgatus* displayed the greatest sensitivity to deoxycholic acid (table S15B). Moreover, the sensitivity of wildtype *B. vulgatus* to 150 μM deoxycholic acid was significantly increased in the presence of 25 μg/mL of the efflux pump inhibitor ($P<0.0001$, one-way ANOVA, Bonferroni multiple comparisons test) (Fig. 6C). In contrast, sensitivity to deoxycholic acid was significantly

reduced in the presence of the same concentration of the inhibitor when *B. vulgatus acrR* was mutated (and expression of the efflux pump was increased) ($P<0.0001$, one-way ANOVA, Bonferroni multiple comparisons test; see Fig. 6C). The effect of the efflux pump was also seen with 250 μM cholic acid, glycocholic acid, and taurocholic acid, where sensitivity was significantly reduced in the mutant compared to wildtype strains in the presence of the inhibitor ($P=0.02$, 0.002 and 0.006, respectively, t-test, Bonferroni correction; table S15B). Complementation of the *B. vulgatus acrR::IN* mutant partially restored sensitivity to deoxycholic acid (Fig. 6C, table S15B).

Compared to wildtype *B. vulgatus*, wildtype *B. dorei* was significantly less sensitive to deoxycholic acid in the presence of PAβN ($P<0.0001$, one-way ANOVA, Bonferroni multiple comparisons test; Fig. 6C), just as it was significantly less sensitive to retinol in the presence of the inhibitor (Fig. 6B). This reduced sensitivity to both compounds could be measured in two ways: by noting the fold-difference in sensitivity of each organism to retinol or deoxycholic acid as a function of treatment with the inhibitor, and by noting the absolute difference in sensitivity values between the organisms in the presence of deoxycholic acid plus the inhibitor or retinol plus the inhibitor. These measures provide one operational definition of the increased efflux capacity of *B. dorei* for these two compounds.

Follow-up electrophoretic mobility shift assays revealed that none of these bile acid species affected the binding of AcrR to its target DNA sequence (fig. S5A), a finding independently confirmed by fluorescence polarization assays, which showed minimal effects on K_d (fig. S5C). Considered together, our findings indicate that these bile acids are not direct regulators of AcrR activity. However, we cannot rule out the possibility that bile acids (or retinol) are metabolized to derivatives that operate as AcrR effectors or on some other pathway or additional regulator that affects AcrR. Our observations also support the notion that *in vivo* dietary retinol availability and bile acid metabolites generated through biotransformation by members of the gut microbiota may interact to influence the fitness of *B. vulgatus* via its AcrAB-TolC efflux system. Moreover, the fact that the *B. vulgatus* AcrAB-TolC1/2 locus did not significantly change its expression *in vivo* as a function of the vitamin A manipulations applied to our gnotobiotic mouse model of the human gut microbiota suggests that the constitutive level of activity of the efflux pump is a key determinant of the sensitivity of *B. vulgatus* compared to other bacterial members of the community (e.g., *B. dorei*) to changes in retinoid availability. However, additional studies are needed before any conclusions can be made about whether the AcrR-mediated resistance to retinol inhibition observed *in vitro* is a critical determinant of the broader reconfiguration of the defined bacterial community that occurs *in vivo*.

Discussion

Deliberate manipulation of dietary iron, folate, zinc or vitamin A produced the unanticipated finding that vitamin A had the greatest effect on the structure and meta-transcriptome of a phylogenetically diverse, defined human gut bacterial community in gnotobiotic mice. Much information has accumulated about the effects of retinoids on host rather than microbial cell biology, including their pivotal role in signal transduction. The current study provides preclinical evidence supporting the concept that the presence and subsequent treatment of

micronutrient imbalances need to be considered from the perspective of not only the human host but also the host's gut microbiota.

As noted above, *B. vulgatus* is one of a number of growth-discriminatory strains identified in a preclinical gnotobiotic mouse model of human gut microbiota development (16). The underrepresentation of some of these growth-discriminatory strains in the gut microbial communities of undernourished children provides a rationale for developing nutritional interventions designed to increase their abundance and expressed beneficial functions (18). While our results establish that vitamin A deficiency increases, and repletion decreases, the representation of *B. vulgatus* in our model community, we lack preclinical or clinical evidence of its contribution to host growth relative to other growth-discriminatory strains in the developing microbiota. As such, we cannot conclude at this time that vitamin A imbalances influence host growth through their effects on *B. vulgatus* specifically (or that an increase in the abundance of this putative growth-promoting taxon in a vitamin A deficient state would represent an adaptive response). However, our results do suggest that the impact of vitamin A dose and pharmacokinetics on this and other growth-discriminatory organisms present in the developing microbiota of children at risk for or with already manifest undernutrition should be evaluated. Studies conducted in gnotobiotic animal models where diet and microbiota composition can be precisely controlled and manipulated provide a useful starting point for addressing this challenging problem. There are formidable problems with directly proceeding to human studies without prior knowledge gleaned from preclinical animal models. These problems include distinguishing primary effects of dietary micronutrient content on the microbiota from host effects, as well as the challenge of stratifying a target human population composed of individuals of varying ages, with varying combinations of micronutrient deficiencies and microbiota compositions, and with varied histories of exposure to supplements containing various combinations and doses of micronutrients.

The current study extends previous work performed with defined human gut communities composed of reference 'domesticated' bacterial strains derived from diverse human donors, to characterize the interactions of specified deliberate dietary nutrient manipulations on the structural and functional features of these artificial microbiota. The diversity of the community described in the present report and the reliability of its installation in gnotobiotic mice represent an advance over our previous gnotobiotic models (32, 45–48). This capacity to reliably assemble a more complex defined model human gut microbiota where all component organisms and their gene content are known, expands our capacity to (i) 'capture' the structural and functional responses of a broader range of community members to a variety of dietary manipulations (e.g. by COPRO-Seq, microbial RNA-Seq, mass spectrometry-based proteomic or metabolomics studies), and (ii) subsequently prioritize further analyses based on the observed effect size and nature of the responses. These studies also illustrate how once such prioritization is made, an informative next step is to construct INSeq libraries from the most responsive taxa and perform *in vitro* screens with identified bioactive dietary compounds to decipher the molecular underpinnings of the observed *in vivo* response. Nonetheless, our experiments illustrate one challenge in characterizing the effects of deliberate perturbations of defined artificial human gut communities with increasing degrees of complexity: while 'consistent' community membership was achieved

across co-housed animals within and across treatment groups based on the criterion of 'presence/absence' and Bray-Curtis dissimilarity measurements, we observed changes in relative abundance over time even in the untreated control group. We accommodated this apparent 'stochasticity' by performing several types of comparisons: (i) a 'within treatment group' comparison where each mouse served as its own control, documenting community structure and meta-transcriptome before, during and after a single type of acute micronutrient deficiency is applied, and where mice were also compared to one another; (ii) a between-group comparison where the responses of a given treatment group were referenced to members of the control group that monotonously consumed a micronutrient-sufficient diet and (iii) in the case of vitamin A, a between-group comparison where the responses to this single dietary micronutrient deficiency were compared to the responses to the multiply deficient diet. The robustness of responses to dietary or other types of manipulations can be examined further in communities with the degree of complexity described in this report, or even greater degrees of complexity, by performing multiple independent experiments with co-housed coprophagic animals.

These approaches set the stage for future studies that apply specified dietary micronutrient deficiencies to gnotobiotic mice of varying ages harboring (i) defined collections of cultured age- and growth-discriminatory human gut bacterial strains representing the different stages of assembly of the human gut microbiota, or (ii) intact uncultured, normally-developing microbiota from children with healthy growth phenotypes, or immature microbiota from those with undernutrition. The results should not only allow further dissection of the mechanisms by which micronutrients interact with community members to shape microbiota and host development, but also may inform new approaches for more effectively treating (and ultimately preventing) the short- and longer-term sequelae of deficiency states. These animal models can also support tests of whether current dosing protocols for micronutrient repletion may have unintended and deleterious effects on the developing microbiota of the very children whose healthy growth such treatments are intended to promote.

Materials and Methods

Study Design

Each experimental group consisted of 5 mice housed in a single cage, with all cages housed in a single gnotobiotic isolator. Groups of mice were age- and weight-matched prior to colonization (see below) and diet treatments were randomly assigned to each experimental group. Experimental diets were custom designed and manufactured by Harlan Teklad/Envigo (Wisconsin, USA). Six diets were produced: four were devoid of one micronutrient (vitamin A, iron, zinc, or folic acid), all four micronutrients were absent in another, and one contained sufficient levels of all of these micronutrients. To design a consistent, defined base diet for all experimental diets, a nutritionally-replete mixture of individual amino acids was used in place of complete protein. Custom vitamin and mineral mixes containing only the micronutrients appropriate to each diet were then added to the base diet to generate each experimental diet. Diets were measured into ~500 g portions, placed into 3 mm thick vacuum-sealed bags (Uline, Inc., Pleasant Prairie, WI), and then put into a second bag that was also vacuum-sealed. Diets were shipped overnight on ice for sterilization by gamma

radiation (20 kGy-50 kGy; STERIS Corp, Mentor, OH). The nutritional characteristics of each irradiated diet were calculated based on diet formulation and are reported in table S1. Investigators were not blinded to diet treatments. All animals studied were included in subsequent analyses.

Bacterial strains and culture conditions

Reference type strains used in this study are listed table S2. Strains were grown in Gut Microbiota Medium (GMM; 49) or on Brain Heart Infusion agar (BHI, Becton-Dickinson, Maryland, USA) supplemented with 10% horse blood, under anaerobic conditions (atmosphere 5% H_2, 20% CO_2, 75% N_2) in a soft-sided plastic anaerobic chamber (Coy Laboratory Products, Michigan, USA). The identity of each strain was confirmed by sequencing full length 16S rRNA gene amplicons generated using the universal primers 8F and 1391R. Strains were arrayed into 96-well format and preserved at −80°C in GMM containing 15% glycerol. Additional manipulations of the arrayed collection were performed inside the anaerobic chamber using a Precision XS liquid-handling robot (Biotek Instruments, Inc.).

A primary human isolate of *Bacteroides vulgatus* (16) was cultured anaerobically in BHI broth supplemented with L-cysteine (0.5g/L), L-histidine (0.2 mM), hematin (1.9 μM) and Vitamin K_3 (1 mg/L) (referred to as BHI+ broth) or on BHI-Blood plates. *Escherichia coli* S17 λpir was used for routine cloning and as a conjugation donor for genetic experiments involving *B. vulgatus*; it was grown in LB-Miller broth or on LB plates (BD Difco). Antibiotics were added to media as appropriate: ampicillin (100 μg/mL), erythromycin (25 μg/mL), tetracycline (2 μg/mL), and gentamicin (200 μg/mL).

Gnotobiotic mouse experiments

All experiments involving mice were performed using protocols approved by the Animal Studies Committee of the Washington University School of Medicine. *Colonization of germ-free mice* - A −80°C stock plate of the clonally-arrayed culture collection was thawed in the anaerobic chamber. A 96-well, deep-well plate (Thermo Scientific Nunc) was filled robotically with 960 μL of GMM broth. A 40 μL aliquot was withdrawn from each well of the culture collection and inoculated into the recipient plate, which was then covered with an atmosphere-permeable seal (VWR). The inoculated plate was incubated under anaerobic conditions for 48 h at 37°C, after which time an aliquot of each well was assayed for growth by measuring OD_{600}. Equal volumes of each well culture were pooled, mixed, transferred to 1.8 mL crimp seal glass vials (Wheaton, NJ, USA) and sealed for transport to the gnotobiotic mouse facility. Vials were immediately fogged into gnotobiotic isolators and 500 μL of the pooled culture was introduced into each recipient germ-free mouse by a single oral gavage.

Adult male CF57BL/6J mice were maintained in a flexible plastic film gnotobiotic isolator and fed a nutritionally-sufficient standard diet (B&K autoclavable chow #7378000, Zeigler Bros Inc.) *ad libitum*. Four days prior to gavage of the defined 92-strain culture collection, all mice were transitioned to the nutritionally-sufficient experimental diet. On experimental day 0, mice received 500 μL of the strain mixture.

All mice were maintained on a strict light cycle (lights on at 0600h, off at 1800h). All diets were provided *ad libitum*. All animals in all treatment groups were observed on a daily basis and weighed weekly. Autoclaved bedding (Aspen woodchips; Northeastern Products) was changed weekly and at the beginning of each diet oscillation.

The timing of fecal sampling for COPRO-Seq and microbial RNA-Seq analyses is described in Fig. 1A. All fecal samples were collected from individual mice into 2 mL screw cap tubes (Axygen, CA, USA). Once sampling of the animals in an isolator had been completed, tubes were removed promptly and snap-frozen in liquid N_2, after which time they were transferred to a −80°C freezer.

Community Profiling by Sequencing (COPRO-Seq)

The microbial community structure in each fecal sample was analyzed by COPRO-Seq (47). Briefly, DNA was isolated by subjecting each fecal pellet (n=5 samples per experimental group, per time point) to bead-beading in a mixture containing 500 μL Buffer A (200 mM NaCl, 1200 mM Tris, 20 mM EDTA), 210 μL 20% SDS, 500 μL phenol:chloroform:isoamyl alcohol (25:24:1, pH 7.9, Ambion) and 250 μL of 0.1 mm zirconium beads (BioSpec Products, OK, USA) for 3 min (Mini-Beadbeater-8; Biospec). The aqueous phase was collected after centrifugation at 4°C for 3 min at 8000 × g, and nucleic acids were purified (Qiaquick columns, Qiagen) and eluted into 10 mM Tris.

COPRO-Seq libraries were prepared by first sonicating 100 μL of a 5 ng/μL solution of DNA from each fecal sample [Bioruptor Pico (Diagenode, Jew Jersey, USA); 10 cycles of 30 sec on / 30 sec off at 4°C]. Fragmented DNA was cleaned up in MinElute 96 UF PCR Purification plates (Qiagen). The fragments were blunt-ended, an A-tail was added, and the reaction products were ligated to Illumina paired-end sequencing adapters containing sample-specific 8 bp barcodes. Size selection was performed (1% agarose gels); 250–350 bp fragments were excised and the DNA purified by MinElute Gel Extraction (Qiagen). Adapter-linked fragments were enriched by a 20-cycle PCR using Illumina PCR Primers PE 1.0 and 2.0 followed by MinElute PCR Purification (Qiagen); if agarose gels indicated adapter dimers an additional size-selection was performed (AMPure XP SPRI bead cleanup; Beckman Coulter, California, USA). Libraries were pooled and sequenced using Illumina MiSeq or HiSeq instruments (unidirectional 50 nt reads).

Sequence data were de-multiplexed and mapped to the reference genomes of community members plus three “distractor” genomes (*B. fragilis* NCTC 9343, *Clostridium perfringens* ATCC 13124, and *Shigella* sp. D9). The proportion of reads mapping to the “distractor” genomes was used to set a minimum count threshold cutoff indicating the presence/absence of an organism in the community on a per-sample basis. Normalized counts for each bacterial strain in each sample were used to produce a relative abundance table (summarized in table S3). Prior to statistical analyses, the table was further filtered to exclude organisms not present at 0.1% relative abundance in >25% of samples collected.

To identify bacterial taxa whose relative abundances were influenced by the micronutrient deficiency treatments, we rarefied the abundance table to 7,000 reads per sample and used linear mixed-effects models of log-transformed abundances (plus one pseudo-count). For

each taxon, models were generated for each of the five dietary micronutrient deficiencies, including the micronutrient sufficient group as a control in each model. Each model included (i) experimental stage (end of first sufficient diet phase at experimental day 14; 14 days after initiation of the micronutrient deficient diets; 14 days after return to the sufficient diet), (ii) treatment group (deficiency versus control) and (iii) their interaction as fixed effects, with individual mice treated as a random effect. A significant interaction term was considered evidence of a potentially interesting influence of the micronutrient deficiency, and tests of differences of least-squares means between the control and deficiency groups in each experimental stage, followed by *P*-value adjustments using Holm's method, were used to further explore the effects of the experimental treatments.

In addition, relative abundances before and after diet oscillation were compared using the group_significance.py script in QIIME version 1.9.0 (50). A follow-up analysis was performed in R (version 3.2.3; 51). Relative abundance data and associated metadata files were read into R, and the change in relative abundance for each organism within an individual mouse between two diet phases was calculated. These values were compared across experimental groups to identify changes in relative abundance that were significantly different from relative abundance responses in other experimental groups. For all univariate analyses, both nonparametric and parametric statistical tests were performed and the results compared.

Microbial RNA-Seq

Triplicate cultures of wildtype *B. vulgatus* and isogenic mutants were diluted 1:100 from overnight cultures into 5 mL of fresh *Bacteroides* defined medium (BDM; prepared by mixing equal volumes of a 2× concentrate of the carbohydrate-free medium stock with a 2× concentrated carbon source solution, as described previously; 48), and grown to mid-log phase (OD_{600} 0.4–0.6) under anaerobic conditions in sealed Balch tubes. Once cultures reached mid-log phase, they were treated with RNAProtect Bacteria Reagent (Qiagen), vortexed, and incubated at room temperature for 5 minutes. Cultures were then transferred to clean 15 mL tubes, centrifuged for 10 min at 3023 × g, supernatants were decanted, and the pellets were stored at −80°C. Both cryopreserved *in vitro* cultures and fecal pellets (n=3 samples per experimental group, per time point) obtained from mice were thawed and resuspended in 500 μL of Buffer A immediately prior to extraction of total RNA.

Microbial RNA-Seq was performed as previously described (45, 47, 48). Following acid phenol extraction, precipitation in isopropanol, and two rounds of DNAse treatment [each followed by cleanup using a MEGAClear column (Ambion)], RNA integrity was confirmed by gel electrophoresis and PCR-based checks for genomic DNA contamination were performed. 23S rRNA, 16S rRNA, 5S rRNA and tRNA were removed [Ribo-Zero Kit (Illumina)] and purified bacterial mRNA was precipitated with ethanol in the presence of GlycoBlue (Ambion; used to ensure subsequent complete resuspension in nuclease-free H_2O). Double-stranded cDNA was synthesized using random hexamers and Superscript II (Invitrogen). Illumina library preparation was performed as described above for COPRO-Seq; however, size selection was performed in the 200–300 bp range. Libraries were subjected to sequencing first on the Illumina MiSeq platform for quality control purposes,

after which library balance adjustments were made where necessary and final sequencing at greater depth was performed using the Illumina HiSeq platform (50 nt unidirectional reads).

Data analysis—The pipeline we employed for processing short-read meta-transcriptomic data is described in a previous publication (45). Briefly, sequence data were demultiplexed and bowtie version 1.1.0 (52) was used to map reads to the genomes of community members. Raw counts were subsetted, then normalized and analyzed using DESeq2 (53) in R 3.2.3 employing two complementary strategies ('top-down' and 'bottom-up'). To analyze data at the community level (top-down view of the meta-transcriptome), raw count data for each comparison was filtered at a low abundance threshold of ≥3 raw reads and for consistent representation in biological replicates (present in ≥2 samples in both micronutrient-sufficient and –deficient diet groups compared, or present in all samples in one group and in none of the other), and then imported into R. Size factors and dispersions were estimated in DESeq2. Significant differential expression was defined using the Wald test based on negative binomial model-fitting. To obtain a strain-level view of transcriptional responses (bottom-up analysis), RNA-Seq data were subsetted by strain, filtering for low abundance and sample representation as above, and the resulting dataset analyzed in R using DESeq2. Rarefaction was used to determine the fraction of expressed protein-coding sequences in each organism that was detected across all RNA-Seq samples. Examination of the saturation characteristics of per-strain rarefaction curves across all samples allowed us to stratify organisms by predicted transcriptome saturation. Strains that colonized gnotobiotic mice (by COPRO-Seq analysis) but for which saturation was low (*Bacteroides finegoldii* DSM 17565, *Bacteroides ovatus* ATCC 8483, *Bifidobacterium adolescentis* L2–32, *Enterobacter cancerogenus* ATCC 35316, *Megamonas funiformis* DSM 19343, *Parabacteroides distasonis* ATCC 8503, and *Proteus penneri* ATCC 35198) were excluded from the bottom-up analysis (all transcriptomic data was included in the top-down community-level analysis).

Functional annotation of differentially expressed genes—The general strategy and bioinformatic tools used for functional analysis of microbial RNA-Seq data are described in an earlier publication (47). Predicted protein-coding genes in the genomes of community members were annotated by BLASTP query (e-value threshold of 1E-05) against the Kyoto Encyclopedia of Genes and Genomes (KEGG) database (release 4 January 2016). Annotation results were used to match coding sequence locus tags to KEGG Orthology (KO) identifiers. KO lookup tables for each genome were used to annotate transcriptional data, which were then used to determine the representation of various levels of the KEGG hierarchy, including 'General', 'Categories', 'Pathways', 'Functions' and 'Enzyme Commission numbers' in each RNA-Seq dataset. A more detailed (manual) curation of functional assignments for genes implicated in the predicted AcrR regulon was performed using comparative genomics tools in the SEED database and RAST (Rapid Annotation of microbial genomes using Subsystems Technology) (54).

Pathway enrichment analyses—Hypergeometric enrichment and gene set enrichment analysis (GSEA) were performed using the R packages clusterProfiler (55) and GAGE (56), respectively. Gene set information for both "top-down" (community-wide) and "bottom-up"

(strain-level) analyses were derived from the KEGG-based functional annotations described above. For hypergeometric enrichment tests, the set of differentially-expressed genes (as defined by DESeq2) was supplied to the generalized "enricher" tool in clusterProfiler, along with the corresponding gene set information (i.e. their corresponding KEGG-level functional group). For GSEA, DESeq2-normalized counts were supplied to GAGE along with the corresponding gene set information and with options 'same.dir = F (genes allowed to change expression in different directions),' 'saaTest = gs.KSTest (use non-parametric Kolmogorov-Smirnov test to order genes)', and 'rank.test = F (required for gs.KSTest)'. For both enrichment analyses, *P*-values were adjusted to control false discovery rates by the Benjamini-Hochberg method.

Phenotypic screen for the effects of various retinoids on growth of *Bacteroides spp.*

Stocks (50 mM) of retinol, retinal, retinoic acid, retinyl palmitate, β-carotene, and geranylgeraniol (Sigma-Aldrich) were prepared in dimethyl sulfoxide under low-light conditions and stored in N_2-purged amber vials at −80°C. Bacterial strains were struck from −80°C glycerol stocks onto BHI-blood plates containing antibiotics where appropriate and grown for 48 h at 37°C under anaerobic conditions. Single colonies were picked into BHI+ broth and grown overnight under anaerobic conditions at 37°C. Cultures were diluted to an OD_{600} of 0.05 in fresh BHI+ broth and grown to mid-log phase. Either retinoids or DMSO (vehicle control) were mixed at a 25% overblend concentration into appropriate volumes of BDM, after which 150 μL of each treated medium was aliquoted into wells of a 96-well plate (Techno Plastic Products AG) using a liquid-handling robot housed in the Coy chamber. Mid-log test cultures were subsequently diluted 1:25 into 1 mL BDM/0.02% v/v DMSO in deep-well plates; 50 μL of the diluted cultures were transferred to recipient wells in the test plate by robot, yielding 1× treatment and 1:100 final dilutions of the bacterial strains (n = 3–4 test cultures per treatment per experiment, experiments performed in duplicate unless indicated). Test plates were sealed with optically clear film (Axygen UC500) and transferred to a plate stacker-reader system housed in the anaerobic chamber (BioTek Eon and Biostack 4). For data collection from individual plates, each plate was placed in the Eon plate reader and incubated at 37°C, with OD_{600} values determined at 15 minute intervals. For multiplate data collection, the anaerobic chamber was heated to 37°C and plates were placed in the plate-handling robot and draped with laboratory diapers to achieve low-light conditions; OD_{600} measurements were performed for each plate at 15 minute intervals.

For multidrug efflux inhibitor studies, cultures were prepared as described above for retinoid sensitivity testing and treated with phenylalanine-arginine β-naphthylamide (PAβN, Sigma-Aldrich) at 0 or 25 μg/mL, with or without 10 μM retinol in 200 μL BDM. Plates were sealed and OD_{600} was monitored.

At the conclusion of each experiment, data were exported to text file and in-house perl scripts were used to plot growth curves and calculate growth rate, the time at which each growth curve crossed a user-defined OD_{600} threshold, and the maximum OD_{600} achieved. Curve parameters were normalized to corresponding values from control cultures of the

same strain (in 0.02% DMSO) prior to performing comparisons between strains (Prism 6.0, GraphPad Software).

High resolution quantitative mass spectrometry-based proteomics

Wildtype *B. vulgatus* ATCC 8482 was cultured (n=2 per treatment) in BDM in the presence of 1 μM retinol or vehicle alone (0.02% DMSO), pelleted, and frozen for storage at −80°C. Proteins were extracted, digested with trypsin, and 25 μg peptides were measured across eleven salt-cuts of a 24h MudPIT LC-MS/MS analysis using an Orbitrap Elite MS (48). Resulting MS/MS spectra were searched against the *B. vulgatus* proteome database (concatenated with common contaminants and decoy sequences to assess false-discovery rates) using the Myrimatch v. 2.1 search algorithm (57). Peptide spectrum matches were scored and filtered (peptide-level FDR < 1 %) via IDPicker v. 3.0 (58), assigned matched-ion intensities, and peptide abundance distributions were normalized and assembled to proteins using InfernoRDN, as described previously (59, 60).

INSeq-based identification of *B. vulgatus* mutants that affect retinoid sensitivity

B. vulgatus ATCC 8482 taxon-specific barcodes were introduced into the INSeq mutagenesis vector (pSAM_Bt; 31) by PCR amplification, using the primer pairs described in table S11. Amplification conditions were as follows: initial denaturation at 94°C for 2 min, followed by 25 cycles of denaturation (94°C for 15 sec), annealing (58°C for 30 sec), and amplification (58°C for 90 sec). Vector DNA was digested with KpnI and BamHI, and the linear product was ligated to the PCR amplicon, yielding the barcoded transposon mutagenesis vector. Whole genome transposon mutagenesis of *B. vulgatus* ATCC 8482 was performed using a published protocol (32).

Aliquots of the mutant library were inoculated into BDM containing retinol (10 μM) or 0.02 % DMSO. Triplicate, large volume cultures (250 mL each; starting OD_{600} of 0.05) were incubated anaerobically at 37°C. Aliquots were removed during lag phase and after retinol-selected cultures reached stationary phase. Additionally, a stationary phase aliquot from the primary culture was used to inoculate 250 mL of fresh selection medium. The resulting secondary cultures were sampled in mid-log phase (OD_{600} 0.4–0.6) and at stationary phase.

DNA was isolated from all cultures/time points, and the abundance and genome location of mutants in input, control, and selected samples were determined by INSeq as follows. The *mariner* Tn contains engineered MmeI sites at both of its ends; thus, DNA was digested with MmeI (which cuts 20 bp distal to its recognition site), yielding products with flanking genomic sequence tags at both ends. Ampure XP bead-based and gel-based size selection was used to isolate and purify the products. Custom, indexed Illumina adapters were ligated to these fragments which were then sequenced (Illumina HiSeq platform; 50 nt reads). INSeq reads were mapped to the *B. vulgatus* genome and analyzed (32) to obtain the identity and abundance of each Tn mutant present in the input library and the selected or control libraries.

Retinol-resistant Tn mutants were isolated by plating dilutions of cryopreserved, stationary-phase selected cultures on BHI-blood containing 25 μg/mL erythromycin. Colony PCR

using primer pairs that spanned inserted Tn borders (one genome location-specific primer and one transposon-specific primer in each pair) were used to confirm the identities of mutants. Confirmed colonies were grown overnight in BHI+ and archived as 15% glycerol stocks at −80°C. Retinoid sensitivity experiments were performed as described above using monocultures of isolated Tn mutant strains.

Complementation of *B. vulgatus* Tn mutants

Tn mutants of *B. vulgatus* were complemented using the genomic insertion vector pNBU2_tetQ (40). The coding sequence of *acrR* (*BVU0240*) was amplified by PCR with Phusion HF Master Mix (New England Biolabs, Massachusetts, USA) from purified genomic DNA from wildtype *B. vulgatus*. To drive constitutive expression of complemented genes, a 300 bp region upstream of the *B. vulgatus rpoD* gene (*PrpoD*) was also amplified by PCR. The pNBU2_tetQ backbone was digested with XbaI and PstI; Gibson Assembly (New England Biolabs) was used to assemble *PrpoD* and the *B. vulgatus acrR* coding sequence into the digested vector, yielding pNBU2_tetQ_*PrpoD_acrR* (abbreviated pNBU2_*acrR*). Assembled vectors were transformed into *E. coli* S17 λpir and the assemblies confirmed by junction-spanning PCR. Vectors were mobilized from *E. coli* donor to the corresponding *B. vulgatus* recipient by conjugation. Briefly, overnight cultures of both donor and recipient were inoculated into corresponding rich media with antibiotics where appropriate and grown for 16–20 h at 37°C (*E. coli*, aerobically with shaking at 225 rpm; *B. vulgatus*, anaerobically without shaking). Stationary phase cultures were then serially diluted into fresh medium and incubated for 4 h at 37°C. Cultures of donor and recipient cells with approximately equal optical densities were pelleted by centrifugation, resuspended as a mixture in 1 mL of fresh medium without antibiotics, and plated on BHI-blood agar. After a 24 h incubation under aerobic conditions, the surface of each plate was scraped, resuspended in 5 mL BHI+ liquid, and plated on BHI+ agar with tetracycline (2 μg/mL). After a 48 h incubation under anaerobic conditions, colonies were picked, re-struck on BHI+ agar with tetracycline, and the site of insertion and orientation of introduced genes in selected colonies was verified by PCR and sequencing. Confirmed complemented Tn mutants carrying either the empty pNBU2_tetQ vector or *B. vulgatus* sequences of interest were subjected to retinoid sensitivity assays as described above.

Transcription factor binding site analyses

Analysis of Bacteroides AcrR regulons—We applied an integrative comparative genomics approach to reconstruct the AcrR regulon in *Bacteroides* species (as implemented in the RegPredict Web server, http://regpredict.lbl.gov) (61). This approach combines identification of candidate regulator binding sites with cross-genomic comparison of regulons and functional context analysis of candidate target genes (62). The upstream regions of *BVU0240* and its orthologs in 11 *Bacteroides* genomes (representing a non-redundant set of species excluding closely related strains) were analyzed employing a DNA motif recognition program (the “Discover Profile” procedure implemented in RegPredict) to identify a conserved palindromic DNA motif. After construction of a position-weight matrix for the candidate AcrR binding motif, we searched for additional AcrR-binding sites in the analyzed *Bacteroides* genomes. Finally, we performed a consistency check or cross-species comparison of the predicted AcrR regulons. Scores of candidate binding sites were

calculated as the sum of positional nucleotide weights. The score threshold was defined as the lowest score observed in the training set. The sequence logo for the derived DNA binding motif was drawn using the WebLogo package (63).

Cloning, expression and protein purification of B. vulgatus and B. dorei AcrR-like regulators—Genes encoding orthologous AcrR-like regulators from *B. vulgatus* (BVU0240, $AcrR_{BV}$) and *B. dorei* (BACDOR_00223, $AcrR_{BD}$) were amplified by PCR from genomic DNA using two sets of specific primers containing BamHI and HindIII restriction sites (table S11). A truncated variant of $AcrR_{BV}$ protein ($AcrR^*_{BV}$) that lacks eight N-terminal amino acids was cloned using an alternative forward primer (table S11). This "truncated variant" corresponds to an alternative translational start of this protein as currently reflected in GenBank (WP_008782083.1).

Amplicons specifying the full length AcrR orthologs from *B. vulgatus* and *B. dorei* and the truncated $AcrR^*_{BV}$ variant were cloned into the pSMT3 expression vector. The recombinant proteins were expressed under control of the T7 promoter with an N-terminal His6-Smt3-tag in *E. coli* BL21/DE3 and a Ulp1-cleavable, N-terminal Smt3 polypeptide (64). Cells were grown in LB medium (50 mL) to an OD_{600} of ~1.0 and protein expression was induced with 0.2 mM isopropyl-β-D-thiogalactopyranoside (IPTG). Cell were harvested after 18 h of additional shaking at 20°C.

To purify the recombinant $AcrR_{BV}$, $AcrR^*_{BV}$ and $AcrR_{BD}$ proteins, harvested cells were first re-suspended in 20 mM HEPES buffer (pH 7) containing 100 mM NaCl, 0.03% Brij-35, 2 mM β-mercaptoethanol and 2 mM phenylmethylsulfonyl fluoride (Sigma-Aldrich). Cells were then lysed by incubation with lysozyme (1 mg/mL) for 30 min at 4°C, followed by a freeze-thaw cycle, sonication and centrifugation. Tris-HCl buffer (pH 8) was added to the resulting supernatant (final concentration, 50 mM), which was subsequently loaded onto a Ni-NTA agarose mini-column (0.3 mL, Qiagen). After washing with the starting buffer containing 1 M NaCl and 0.3% Brij-35, bound proteins were eluted with 0.3 mL of the starting buffer containing 300 mM imidazole. Protein size and purity were verified by SDS PAGE. Protein concentration was determined by using the Quick Start Bradford Protein Assay kit (Bio-Rad). The N-terminal His6-Smt3-tag was cleaved off the purified proteins by digestion with Ulp1 protease (overnight incubation at 4°C in a reaction mixture containing 0.07 mg/mL of the protease).

DNA binding assays—Interactions between the purified recombinant transcription factors and their predicted DNA-binding sites were assayed using two techniques: electrophoretic mobility shift assay and fluorescence polarization assay. Single-stranded DNA oligonucleotides were synthesized (table S11). A 40 bp oligonucleotide with a fragment of the promoter region of the *BVU0244* gene contained the predicted 30 bp AcrR-binding site. 5′-biotin-labeled DNA fragments were used for electrophoretic mobility shift assays, while fluorescence polarization assays employed DNA fragments 3′-labeled with 6-carboxyfluorescein (the double-stranded labeled DNA fragments were obtained by annealing the labeled oligonucleotides with unlabeled complementary oligonucleotides at a 1:10 ratio). As a negative control, we used a 41-bp DNA fragment from the *BT0356* gene of

B. thetaiotaomicron VPI-5482; this fragment contains the verified binding site of an unrelated transcriptional regulator, AraR (65).

For electrophoretic mobility shift assays, the target DNA fragment (0.25 nM) was mixed with increasing concentrations of the purified tag-free $AcrR_{BV}$ and $AcrR_{BD}$ proteins in a total reaction volume of 20 μL. The binding buffer contained Tris-HCl 20 mM (pH 8.0), KCl 150 mM, $MgCl_2$ 5 mM, DTT 1 mM, 0.05% NP-40, and 2.5% glycerol. After a 25 min incubation at 37°C, the reaction mixture was subjected to electrophoresis (conditions: native 5% polyacrylamide gels in 0.5X TB; 100 min run time at 90V; room temperature). DNA was electrophoretically transferred onto a Hybond-N^+ membrane (Pierce) and fixed by UV cross-linking. Biotin-labeled DNA was detected with the LightShift chemiluminescent electrophoretic mobility shift assay kit (Pierce).

For fluorescence polarization assays, fluorescently-labeled double-stranded DNA fragments (3 nM) were incubated with the increasing concentrations of the purified tag-free $AcrR_{BV}$ and $AcrR_{BD}$ proteins in triplicate in a 100 μL reaction mixture in 96-well black plates (VWR). The binding buffer contained 20 mM Tris-HCl (pH 7.5) and 100 mM NaCl and the incubation was conducted for 20 min at 24°C. Herring sperm DNA (1 μg) was added to the reaction mixture to suppress non-specific binding. Fluorescence polarization measurements were made using a Beckman multimode plate reader (DTX 880) with excitation and emission filters set at 495 and 520 nm. The fluorescence polarization assay values were determined as previously described (66).

Bile sensitivity assays

The bile acid sensitivities of isogenic WT, *acrR::IN*, and pNBU2_*acrR* complemented strains of *B. vulgatus*, plus wildtype *B. dorei* were assayed using methods analogous to those used for defining their sensitivity to different retinoids. Cultures were grown to stationary phase, then diluted to OD_{600} of ~0.01 in BDM containing 0, 250 μM, or 1 mM of each of glycocholic acid (GCA), taurocholic acid (TCA), cholic acid (CA), deoxycholic acid, β-muricholic acid (βMCA), or tauro-β-muricholic acid (TβMCA), with or without 25 μg/mL PAβN (n=3 cultures per treatment). An additional experiment was performed with 150 μM deoxycholic acid in the presence or absence of the efflux pump inhibitor. Bile species were obtained from Sigma-Aldrich except for βMCA (Steraloids) and TβMCA (Santa Cruz Biotechnology). Assays were performed in a volume of 200 μL in triplicate in 96-well plates.

Targeted ultraperformance liquid chromatography-mass spectrometry (UPLC-MS)

Retinoids—Aliquots of cultures of the WT, *acrR::IN*, and *acrR*-complemented *acrR::IN* strains of *B. vulgatus* were diluted into supplemented BHI medium and grown to stationary phase at 37°C under anaerobic conditions. Cultures were then diluted to an OD_{600} of 0.5 in 10 mL PBS/0.2% w/v cysteine and retinol was added to a final concentration of 10 μM (n = 1–3 cultures per treatment, 3 experiments). At indicated time points, a 500 μL aliquot of each culture was placed into a 1.5 mL tube and cells were pelleted in a microcentrifuge for 3 min at 20,817 × g. The supernatant was withdrawn and transferred to a 1 mL sample vial (Waters, MA, USA), and deuterated (D5) retinol (Toronto Research Chemicals, Ontario,

Canada) was added to a final concentration of 10 μM as a spike-in control. Mass spectrometry analyses were performed using an Acquity I Class UPLC system (Waters, MA, USA) coupled to an LTQ-Orbitrap Discovery (Thermo Scientific, MA, USA). Mobile phases for positive ionization were (A) 0.1% formic acid in water and (B) 0.1% formic acid in acetonitrile. Retinol quantification was achieved by comparing measured values to standard curves generated from stocks of retinol and D5-retinol.

Bile acids—UPLC-MS analysis of fecal bile acids was performed using protocols described in an earlier report (43).

Statistical analyses

Routine statistical analyses were performed in R (version 3.2.3) or in Prism 6.0 as indicated. $P < 0.05$ was considered statistically significant after appropriate correction for multiple hypothesis testing. Specific statistical tests and P value corrections are noted throughout the text, in figure legends, and in Supplementary Materials.

Supplementary Material

Refer to Web version on PubMed Central for supplementary material.

Acknowledgments

We thank David O'Donnell, Maria Karlsson and Sabrina Wagoner for their assistance with gnotobiotic mouse husbandry; Barb Mickelson at Envigo for her guidance in designing experimental diets; and Ansel Hsaio and Eric Martens for providing suggestions and reagents for genetic manipulation of *B. vulgatus*.

Funding: This work was supported in part by a grant from the NIH (DK30292). D.A.R. was supported by the Russian Science Foundation (Grant 14-14-00289).

References

1. Bailey RL, WestJr KP, Black RE. The Epidemiology of global micronutrient deficiencies. Ann Nutr Metab. 2015; 66:22–33.
2. Howson, CP., Kennedy, ET., Horwitz, A. Institute of Medicine (US) Committee on Micronutrient Deficiencies. Prevention of Micronutrient Deficiencies: Tools for Policymakers and Public Health Workers. 1998.
3. Black RE, Allen LH, Bhutta ZA, Caulfield LE, de Onis M, Ezzati M, Mathers C, Rivera J. Maternal and child undernutrition: global and regional exposures and health consequences. Lancet. 2008; 371:243–260. [PubMed: 18207566]
4. Underwood BA. Hypovitaminosis A: international programmatic issues. J Nutr. 1994; 124:1467S–1472S. [PubMed: 8064405]
5. World Health Organization. Guideline: vitamin A supplementation in infants and children 6–59 months of age. Geneva: World Health Organization; 2011.
6. Harrison EH. Enzymes catalysing the hydrolysis of retinyl esters. BBA-Lipid Lipid Met. 1993; 1170:99–108.
7. Mayo-Wilson E, Imdad A, Herzer K, Yakoob MY, Bhutta ZA. Vitamin A supplements for preventing mortality, illness, and blindness in children aged under 5: systematic review and meta-analysis. Brit Med J. 2011; 343:d5094. [PubMed: 21868478]
8. Salam RA, MacPhail C, Das JK, Bhutta ZA. Effectiveness of Micronutrient Powders (MNP) in women and children. BMC Public Health 13 Suppl. 2013; 3:S22.

9. Gera T, Sachdev HPS. Effect of iron supplementation on incidence of infectious illness in children: systematic review. Brit Med J. 2002; 325:1142. [PubMed: 12433763]
10. Jaeggi T, Kortman GAM, Moretti D, Chassard C, Holding P, Dostal A, Boekhorst J, Timmerman HM, Swinkels DW, Tjalsma H, Njenga J, Mwangi A, Kvalsvig J, Lacroix C, Zimmermann MB. Iron fortification adversely affects the gut microbiome, increases pathogen abundance and induces intestinal inflammation in Kenyan infants. Gut. 2014; 64:731–742. [PubMed: 25143342]
11. Sazawal S, Black RE, Ramsan M, Chwaya HM, Stoltzfus RJ, Dutta A, Dhingra U, Kabole I, Deb S, Othman M, Kabole FM. Effects of routine prophylactic supplementation with iron and folic acid on admission to hospital and mortality in preschool children in a high malaria transmission setting: community-based, randomised, placebo-controlled trial. Lancet. 2006; 367(9505):133–143. [PubMed: 16413877]
12. Veenemans J, Milligan P, Prentice AM, Schouten LRA, Inja N, van der Heijden AC, de Boer LCC, Jansen EJS, Koopmans AE, Enthoven WTM, Kraaijenhagen RJ, Demir AY, Uges DRA, Mbugi EV, Savelkoul HFJ, Verhouf H. Effect of supplementation with zinc and other micronutrients on malaria in Tanzanian children: a randomised trial. PLoS Med. 2011; 8:e1001125. [PubMed: 22131908]
13. Drakesmith H, Prentice AM. Hepcidin and the iron-infection axis. Science. 2012; 338:768–772. [PubMed: 23139325]
14. Soofi S, Cousens S, Iqbal SP, Akhund T, Khan J, Ahmed I, Zaidi AKM, Bhutta ZA. Effect of provision of daily zinc and iron with several micronutrients on growth and morbidity among young children in Pakistan: a cluster-randomised trial. Lancet. 2013; 382:29–40. [PubMed: 23602230]
15. Subramanian S, Huq S, Yatsunenko T, Haque R, Mahfuz M, Alam MA, Benezra A, DeStefano J, Meier MF, Muegge BD, Barratt MJ, Zhang Q, Province MA, Petri WA, Ahmed T, Gordon JI. Persistent gut microbiota immaturity in malnourished Bangladeshi children. Nature. 2014; 509:417–421.
16. Blanton LV, Charbonneau MR, Salih T, Barratt MJ, Venkatesh S, Ilkaveya O, Subramanian S, Manary MJ, Trehan I, Jorgensen JM, Fan Y, Henrissat B, Leyn SA, Rodionov DA, Osterman AL, Maleta KM, Newgard CB, Ashorn P, Dewey KG, Gordon JI. Gut bacteria that prevent growth impairments transmitted by microbiota from malnourished children. Science. 2016; 351:aad3311. [PubMed: 26912898]
17. Planer JD, Peng Y, Kau AL, Blanton LV, Ndao IM, Tarr PI, Warner BB, Gordon JI. Development of the gut microbiota and mucosal IgA responses in twins and gnotobiotic mice. Nature. 2016; 534:263–266. [PubMed: 27279225]
18. Blanton LV, Barratt MJ, Charbonneau MR, Ahmed T, Gordon JI. Childhoodundernutrition, the gut microbiota, and microbiota-directed therapeutics. Science. 2016; 352:1533. aad9359. [PubMed: 27339978]
19. Mandal S, Godfrey KM, McDonald D, Treuren WV, Bjørnholt JV, Midtvedt T, Moen B, Rudi K, Knight R, Brantsæter AL, Peddada SD, Eggesbø M. Fat and vitamin intakes during pregnancy have stronger relations with a pro- inflammatory maternal microbiota than does carbohydrate intake. Microbiome. 2016; 4:1–11. [PubMed: 26739322]
20. Reddy BS, Pleasants JR, Zimmerman DR, Wostmann BS. Iron and copper utilization in rabbits as affected by diet and germfree status. J Nutr. 1965; 87:189–196. [PubMed: 5834325]
21. Reddy BS, Pleasants JR, Wostmann BS. Effect of intestinal microflora on iron and zinc metabolism, and on activities of metalloenzymes in rats. J Nutr. 1972; 102:101–107. [PubMed: 5007106]
22. Bieri JG, McDaniel EG, Rogers WE. Survival of germfree rats without vitamin A. Science. 1969; 163:574–575. [PubMed: 5762186]
23. Rogers WE, Bieri JG, McDaniel EG. Vitamin A deficiency in the germfree state. Fed Proc. 1971; 30:1773–1778. [PubMed: 4942051]
24. Smith JC, McDaniel EG, McBean LD, Doft FS, Halsted JA. Effect of microorganisms upon zinc metabolism using germfree and conventional rats. J Nutr. 1972; 102:711–719. [PubMed: 5028665]
25. Biesalski HK. Nutrition meets the microbiome: micronutrients and the microbiota. Ann NY Acad Sci. 2016; 1372:53–64. [PubMed: 27362360]

26. Carrothers JM, York MA, Brooker SL, Lackey KA, Williams JE, Shafii B, Price WJ, Settles ML, McGuire MA, McGuire MK. Fecal microbial community structure is stable over time and related to variation in macronutrient and micronutrient intakes in lactating women. J Nutr. 2015; 145:2379–2388. [PubMed: 26311809]
27. Lee T, Clavel T, Smirnov K, Schmidt A, Lagkouvardos I, Walker A, Lucio M, Michalke B, Schmitt-Kopplin P, Fedorak R, Haller D. Oral versus intravenous iron replacement therapy distinctly alters the gut microbiota and metabolome in patients with IBD. Gut. 2016 pii: gutjnl-2015-309940.
28. Werner T, Wagner SJ, Martínez I, Walter J, Chang J-S, Clavel T, Kisling S, Schuemann K, Haller D. Depletion of luminal iron alters the gut microbiota and prevents Crohn's disease-like ileitis. Gut. 2011; 60:325–333. [PubMed: 21076126]
29. Liu L, Tang X-H, Gudas LJ. Homeostasis of retinol in lecithin: retinol acyltransferase gene knockout mice fed a high retinol diet. Biochem Pharmacol. 2008; 75:2316–2324. [PubMed: 18455147]
30. Hernandez-Alvarez E, Pérez-Sacristán BI, Blanco-Navarro I, Donoso-Navarro E, Silvestre-Mardomingo RA, Granado-Lorencio F. Analysis of microsamples of human faeces: a non-invasive approach to study the bioavailability of fat-soluble bioactive compounds. Eur J Nutr. 2015; 54:1371–1378. [PubMed: 26026480]
31. Goodman AL, McNulty NP, Zhao Y, Leip D, Mitra RD, Lozupone CA, Knight R, Gordon JI. Identifying genetic determinants needed to establish a human gut symbiont in its habitat. Cell Host Microbe. 2009; 6:279–289. [PubMed: 19748469]
32. Wu M, McNulty NP, Rodionov DA, Khoroshkin MS, Griffin NW, Cheng J, Latreille P, Kerstetter RA, Terrapon N, Henrissat B, Osterman AL, Gordon JI. Genetic determinants of *in vivo* fitness and diet responsiveness in multiple human gut *Bacteroides*. Science. 2015; 350:aac5992. [PubMed: 26430127]
33. Crowell DN, Anderson MS, Raetz CR. Molecular cloning of the genes for lipid A disaccharide synthase and UDP-N-acetylglucosamine acyltransferase in *Escherichia coli*. J Bacteriol. 1986; 168:152–159. [PubMed: 3531165]
34. Ma D, Cook DN, Alberti M, Pon NG, Nikaido H, Hearst JE. Molecular cloning and characterization of acrA and acrE genes of *Escherichia coli*. J Bacteriol. 1993; 175:6299–6313. [PubMed: 8407802]
35. Zgurskaya HI, Nikaido H. Bypassing the periplasm: reconstitution of the AcrAB multidrug efflux pump of Escherichia coli. Proc Natl Acad Sci USA. 1999; 96:7190–7195. [PubMed: 10377390]
36. Du D, Wang Z, James NR, Voss JE, Klimont E, Ohene-Agyei T, Venter H, Chiu W, Luisi BF. Structure of the AcrAB-TolC multidrug efflux pump. Nature. 2014; 509:512–515. [PubMed: 24747401]
37. Kim J-S, Jeong H, Song S, Kim H-Y, Lee K, Hyun J, Ha N-C. Structure of the tripartite multidrug efflux pump AcrAB-TolC suggests an alternative assembly mode. Mol Cells. 2015; 38:180–186. [PubMed: 26013259]
38. Ma D, Alberti M, Lynch C, Nikaido H, Hearst JE. The local repressor AcrR plays a modulating role in the regulation of acrAB genes of *Escherichia coli* by global stress signals. Mol Microbiol. 1996; 19:101–112. [PubMed: 8821940]
39. Raczkowska A, Trzos J, Lewandowska O, Nieckarz M, Brzostek K. Expression of the AcrAB Components of the AcrAB-TolC multidrug efflux pump of *Yersinia enterocolitica* is subject to dual regulation by OmpR. PLoS ONE. 2015; 10:e0124248. [PubMed: 25893523]
40. Martens EC, Chiang HC, Gordon JI. Mucosal glycan foraging enhances fitness and transmission of a saccharolytic human gut bacterial symbiont. Cell Host Microbe. 2008; 4:447–457. [PubMed: 18996345]
41. Renau TE, Léger R, Flamme EM, Sangalang J, She MW, Yen R, Gannon CL, Griffith D, Chamberland S, Lomovskaya O, Hecker SJ, Lee VJ, Ohta T, Nakayama K. Inhibitors of efflux pumps in *Pseudomonas aeruginosa* potentiate the activity of the fluoroquinolone antibacterial Levofloxacin. J Med Chem. 1999; 42:4928–4931. [PubMed: 10585202]
42. Sayin SI, Wahlström A, Felin J, Jäntti S, Marschall H-U, Bamberg K, Angelin B, Hyötyläinen T, Orešič M, Bäckhed F. Gut microbiota regulates bile acid metabolism by reducing the levels of

tauro-beta-muricholic acid, a naturally occurring FXR antagonist. Cell Metab. 2013; 17:225–235. [PubMed: 23395169]

43. Dey N, Wagner VE, Blanton LV, Cheng J, Fontana L, Haque R, Ahmed T, Gordon JI. Regulators of gut motility revealed by a gnotobiotic model of diet-microbiome interactions related to travel. Cell. 2015; 163:95–107. [PubMed: 26406373]
44. Thanassi DG, Cheng LW, Nikaido H. Active efflux of bile salts by Escherichia coli. J Bacteriol. 1997; 179:2512–2518. [PubMed: 9098046]
45. Rey F, Faith JJ, Bain J, Muehlbauer M, Stevens R, Newgard C, Gordon JI. Dissecting the *in vivo* metabolic potential of two human gut acetogens. J Biol Chem. 2010; 285:22082–22090. [PubMed: 20444704]
46. Faith JJ, McNulty NP, Rey FE, Gordon JI. Predicting a human gut microbiota's response to diet in gnotobiotic mice. Science. 2011; 333:101–104. [PubMed: 21596954]
47. McNulty NP, Yatsunenko T, Hsiao A, Faith JJ, Muegge BD, Goodman AL, Henrissat B, Oozeer R, Cools-Portier S, Gobert G, Chervaux C, Knights D, Lozupone CA, Knight R, Duncan AE, Bain JR, Muehlbauer MJ, Newgard CB, Heath AC, Gordon JI. The impact of a consortium of fermented milk strains on the gut microbiome of gnotobiotic mice and monozygotic twins. Sci Transl Med. 2011; 3:106ra106–106ra106.
48. McNulty NP, Wu M, Erickson AR, Martens EC, Pudlo NA, Muegge BD, Henrissat B, Hettich RL, Gordon JI. Effects of diet on resource utilization by a defined model human gut microbiota containing *Bacteroides cellulosilyticus* WH2, a symbiont with an extensive glycobiome. PLoS Biol. 2013; 11:e1001637. [PubMed: 23976882]
49. Goodman AL, Kallstrom G, Faith JJ, Reyes A, Moore A, Dantas G, Gordon JI. Extensive personal human gut microbiota culture collections characterized and manipulated in gnotobiotic mice. P Natl Acad Sci USA. 2011; 108:6252–6257.
50. Caporaso JG, Kuczynski J, Stombaugh J, Bittinger K, Bushman FD, Costello EK, Fierer N, Peña AG, Goodrich JK, Gordon JI, Huttley GA, Kelley ST, Knights D, Koenig JE, Ley RE, Lozupone CA, McDonald D, Muegge BD, Pirrung M, Reeder J, Sevinsky JR, Turnbaugh PJ, Walters WA, Widmann J, Yatsunenko T, Zaneveld J, Knight R. QIIME allows analysis of high-throughput community sequencing data. Nat Meth. 2010; 7:335–336.
51. R Core Team. R Foundation for Statistical Computing. Vienna, Austria: 2015. R: A language and environment for statistical computing. URL https://www.R-project.org/
52. Langmead B, Trapnell C, Pop M, Salzberg SL. Ultrafast and memory-efficient alignment of short DNA sequences to the human genome. Genome Biol. 2009; 10:R25. [PubMed: 19261174]
53. Love MI, Huber W, Anders S. Moderated estimation of fold change and dispersion for RNA-seq data with DESeq2. Genome Biol. 2014; 15:550. [PubMed: 25516281]
54. Overbeek R, Olson R, Pusch GD, Olsen GJ, Davis JJ, Disz T, Edwards RA, Gerdes S, Parrello B, Shukla M, Vonstein V, Wattam AR, Xia F, Stevens R. The SEED and the Rapid Annotation of microbial genomes using Subsystems Technology (RAST). Nucleic Acids Res. 2013; 42:D206–D214. [PubMed: 24293654]
55. Yu G, Wang L-G, Han Y, He Q-Y. clusterProfiler: an R package for comparing biological themes among gene clusters. OMICS. 2012; 16:284–287. [PubMed: 22455463]
56. Luo W, Friedman M, Shedden K, Hankenson K, Woolf P. GAGE: Generally Applicable Gene Set Enrichment for Pathways Analysis. BMC Bioinf. 2009; 10:161.
57. Tabb DL, Fernando CG, Chambers MC. MyriMatch: highly accurate tandem mass spectral peptide identification by multivariate hypergeometric analysis. J Proteome Res. 2007; 6(2):654–661. [PubMed: 17269722]
58. Ma ZQ, Dasari S, Chambers MC, Litton MD, Sobecki SM, Zimmerman LJ, Halvey PJ, Schilling B, Drake PM, Gibson BW, Tabb DL. IDPicker 2.0: Improved protein assembly with high discrimination peptide information filtering. J Proteome Res. 2009; 8(8):3872–3781. [PubMed: 19522537]
59. Xu Q, Resch MG, Podkaminer K, Yang S, Baker JO, Donohoe BS, Wilson C, Klingeman DM, Olson DG, Decker SR, Giannone RJ, Hettich RL, Brown SD, Lynd LR, Bayer EA, Himmel ME, Bomble YJ. Dramatic performance of Clostridium thermocellum explained by its wide range of cellulose modalities. Sci Adv. 2016; 2(2):e1501254. [PubMed: 26989779]

60. Taverner T, Karpievitch YV, Polpitiya AD, Brown JN, Dabney AR, Anderson GA, Smith RD. DanteR: an extensible R-based tool for quantitative analysis of -omics data. Bioinformatics. 2012; 28(18):2404–2406. [PubMed: 22815360]

61. Novichkov PS, Rodionov DA, Stavrovskaya ED, Novichkova ES, Kazakov AE, Gelfand MS, Arkin AP, Mironov AA, Dubchak I. RegPredict: an integrated system for regulon inference in prokaryotes by comparative genomics approach. Nucleic Acids Res. 2010; 38(Web Server issue):W299–307. [PubMed: 20542910]

62. Rodionov DA. Comparative genomic reconstruction of transcriptional regulatory networks in bacteria. Chem Rev. 2007; 107:3467–3497. [PubMed: 17636889]

63. Crooks GE, Hon G, Chandonia J-M, Brenner SE. WebLogo: a sequence logo generator. Genome Res. 2004; 14:1188–1190. [PubMed: 15173120]

64. Mossessova E, Lima CD. Ulp1-SUMO crystal structure and genetic analysis reveal conserved interactions and a regulatory element essential for cell growth in yeast. Mol Cell. 2000; 5:865–876. [PubMed: 10882122]

65. Chang C, Tesar C, Li X, Kim Y, Rodionov DA, Joachimiak A. A novel transcriptional regulator of L-arabinose utilization in human gut bacteria. Nucleic Acids Res. 2015; 43:10546–10559. [PubMed: 26438537]

66. Ravcheev DA, Li X, Latif H, Zengler K, Leyn SA, Korostelev YD, Kazakov AE, Novichkov PS, Osterman AL, Rodionov DA. Transcriptional regulation of central carbon and energy metabolism in bacteria by redox-responsive repressor Rex. J Bacteriol. 2012; 194:1145–1157. [PubMed: 22210771]

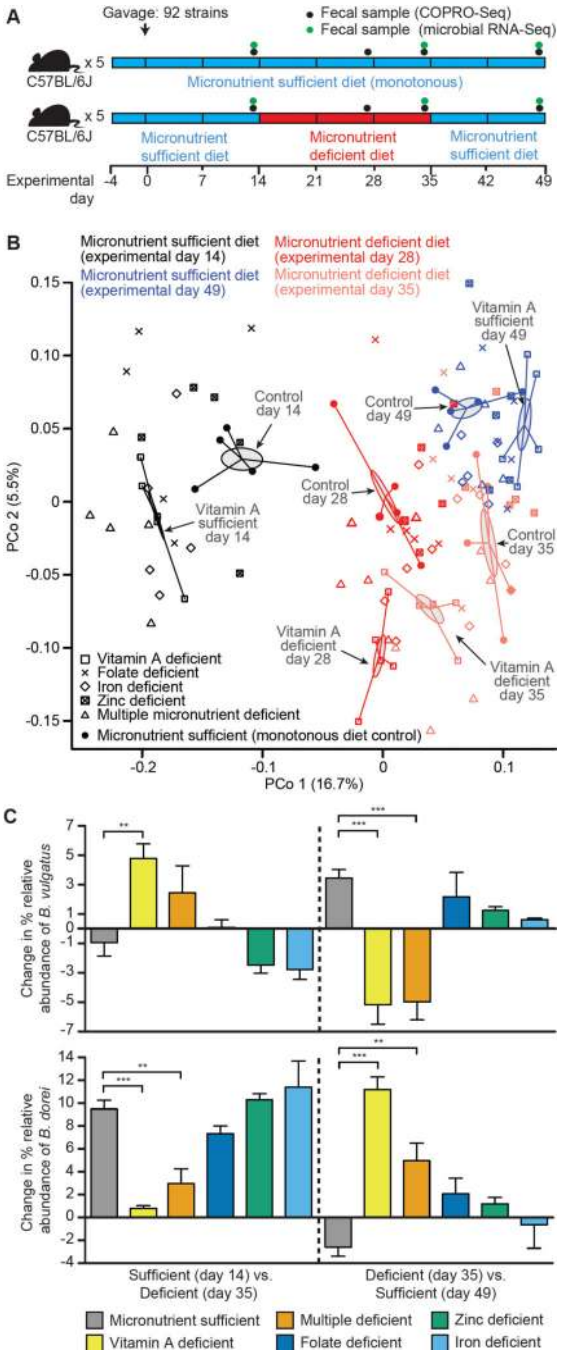

Fig. 1. The effect of dietary micronutrient deficiency on the configuration of a defined human gut microbiota established in gnotobiotic mice

(**A**) Experimental design. (**B**) Principal Coordinates Analysis (PCoA) of pairwise comparisons of fecal microbiota using Bray-Curtis dissimilarities of Wisconsin square root-transformed abundance data obtained from COPRO-Seq analysis. Fecal samples were obtained from mice in the indicated treatment groups at the indicated time points. Gray-shaded ellipses and spokes indicate the standard error of sample group centroids from the vitamin A-deficient and the micronutrient sufficient (monotonous diet control) groups in

each experimental phase. (**C**) COPRO-Seq analysis of the effects of the micronutrient-deficient versus sufficient diets on the abundance of *B. vulgatus* and *B. dorei* in the fecal microbiota of gnotobiotic mice. Mean values ± SEM are shown. **, $P<0.01$; ***, $P<0.001$ (one-way ANOVA, Tukey's Honest Significant Difference (HSD), False Discovery Rate (FDR) correction; $n=5$ mice/treatment group).

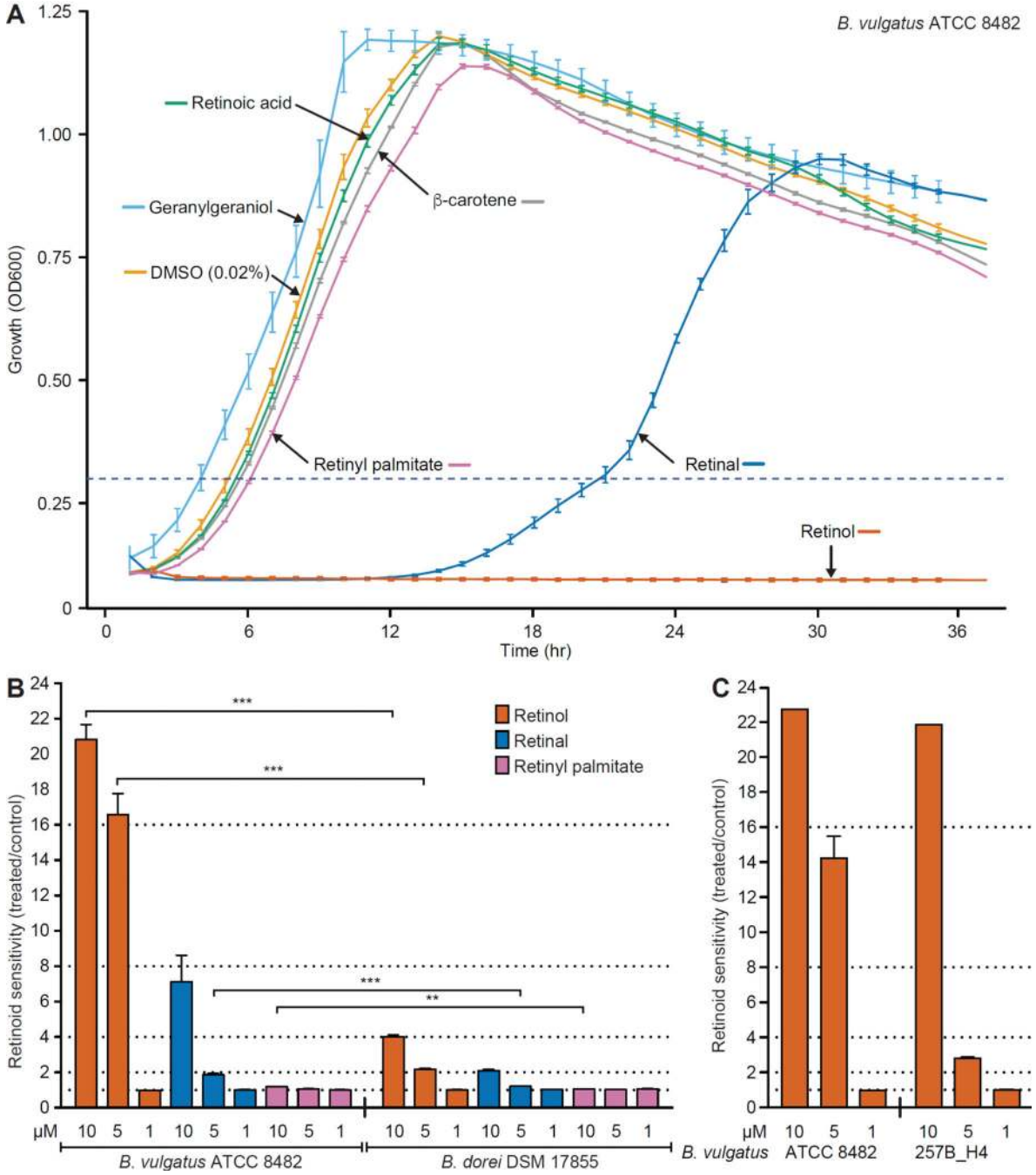

Fig. 2. The distinct retinol sensitivity phenotypes of *B. vulgatus* strains and *B. dorei in vitro*

(**A**) Growth curves of *B. vulgatus* in defined medium with and without various retinoids. The horizontal dashed line indicates the threshold used for calculating time-to-log phase measurements. (**B,C**) Bar plots indicating mean (± SEM) retinoid sensitivity, calculated as time-to-log phase for treated cultures versus time-to-log phase for vehicle alone (DMSO) control cultures for (**B**) *B. vulgatus* ATCC 8482 versus *B. dorei* DSM 17855 or (**C**) *B. vulgatus* strain ATCC 8482 versus *B. vulgatus* strain 257_H4 isolated from a healthy Malawian infant (16). For example, the sensitivity value of 20.8±2.1 for wildtype *B.*

vulgatus incubated in medium containing 10 μM retinol in panel B was calculated by dividing the total incubation period (in this case 95 h) by the time required for vehicle alone-treated control cultures of the same strain to cross the OD_{600} threshold of 0.3. Mean values ± SEM are shown except under those conditions in panel C where the concentration of retinol tested completely inhibited growth. $n=2$ independent experiments, each in triplicate for panel B and one experiment performed in triplicate for panel C. *$P<0.05$, **, $P<0.01$, ***, $P<0.001$ (one-way ANOVA, Bonferroni multiple comparisons test).

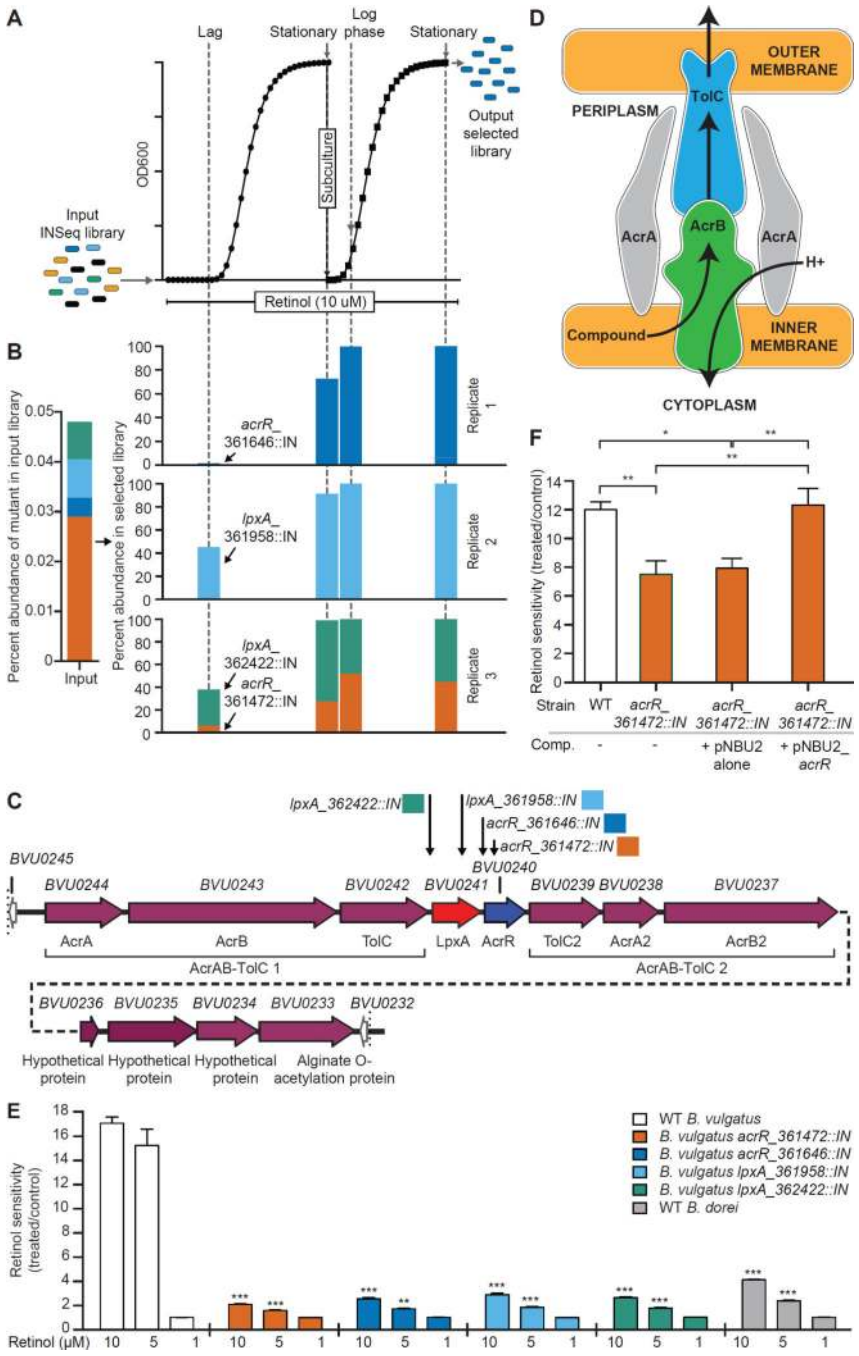

Fig. 3. Selection of retinol-resistant *B. vulgatus* Tn mutants

(**A**) Experimental design. The mutant library was inoculated into defined medium containing 10 μM retinol or 0.02% v/v DMSO (three cultures per treatment). In the first round of selection, mutant libraries were allowed to grow to stationary phase and were then passaged to fresh medium and subjected to a second round of selection. Aliquots were withdrawn in lag and stationary phases from the primary cultures and in log and stationary phases of the secondary cultures. The site of insertion of the Tn was defined in the retinol-resistant mutants using INSeq. (**B**) Percent abundance of Tn mutants in retinol-selected *B. vulgatus*

libraries. The left portion of the panel indicates the abundance of each selected mutant in the input library. Each set of four bars shown in the right portion of the panel indicates the abundance of the Tn mutants at the indicated growth phases from both primary and passaged cultures. (**C**) Schematic of the *B. vulgatus* locus containing the retinol-resistant mutants identified from screening the Tn library. Annotation is based on the NCBI reference assembly NC_009614.1. The genomic location of each selected Tn mutant is indicated by a downward pointing arrow annotated with the corresponding color from panel **B** and the corresponding genome coordinate for the site of Tn insertion. (**D**) Schematic of components comprising the *E. coli* AcrAB-TolC efflux system (adapted from http://2013.igem.org/Team:Ciencias-UNAM/Project). (**E**) Retinol sensitivity of *B. vulgatus* wildtype (WT) and Tn mutants grown in monoculture in defined medium treated with 1 μM, 5 μM, and 10 μM retinol versus 0.02% v/v DMSO as a reference vehicle control. Mean values ± SEM of the ratio between treated and control cultures for each strain are shown. The sensitive *B. vulgatus* wildtype strain and resistant *B. dorei* wildtype strain are shown as positive and negative controls, respectively. (**F**) Retinol (10 μM) sensitivity of the wildtype, *acrR::IN* (genome location 361472) mutant, and complemented *B. vulgatus acrR::IN* + pNBU2_*acrR* mutant strains (abbreviated Comp), plus a control *B. vulgatus acrR::IN* strain containing the empty vector. The results shown in panel E are from two independent experiments, each performed in triplicate, while those in panel F are from three independent experiments each performed in triplicate or quadruplicate. *$P<0.05$, **, $P<0.01$, ***, $P<0.001$ (one-way ANOVA, Bonferroni multiple comparisons test).

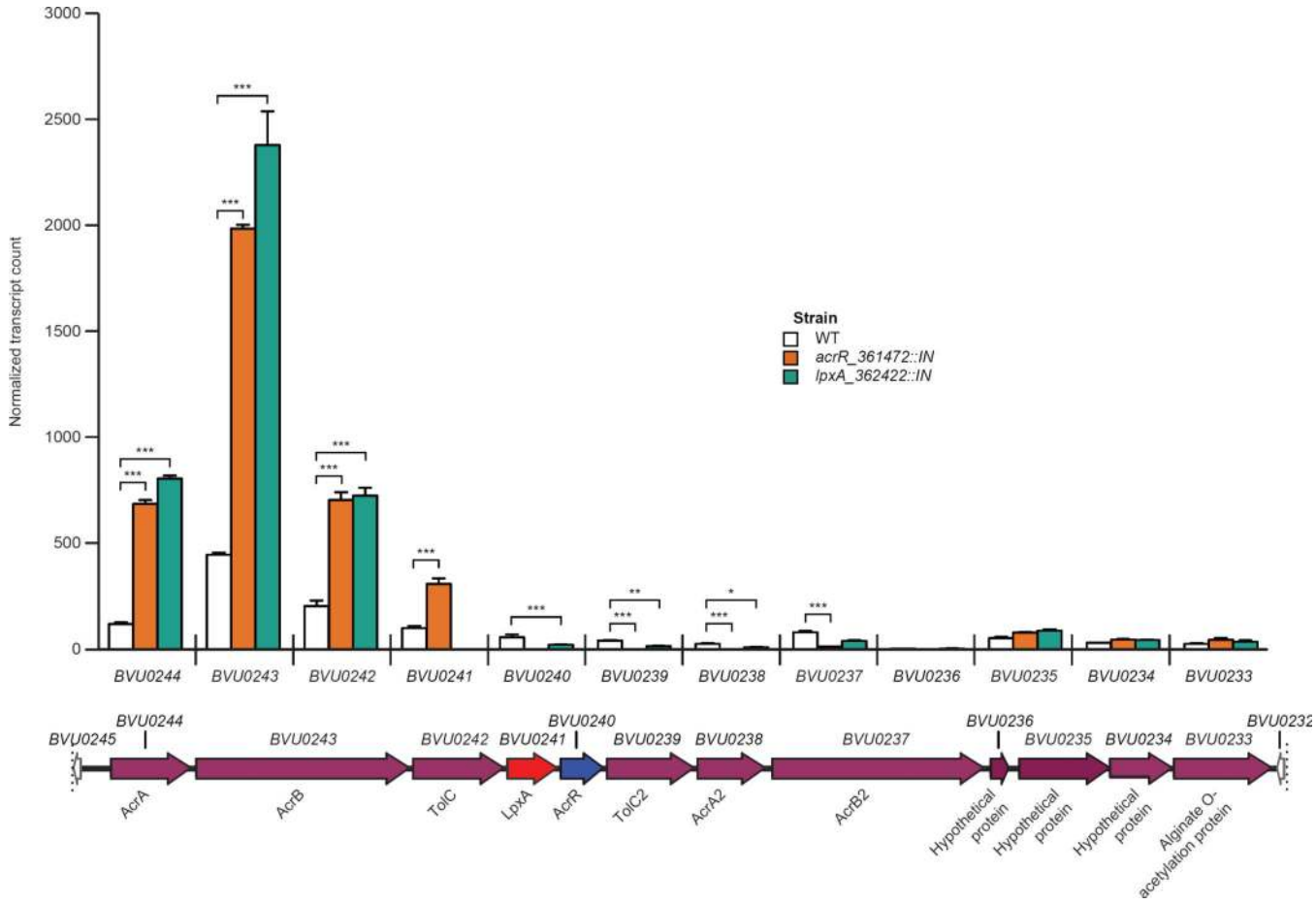

Fig. 4. Transcriptional response of the *B. vulgatus* locus containing the AcrAB-TolC efflux pump to insertional mutagenesis of *acrR* or *lpxA*

Microbial RNA-Seq analysis of gene expression in mid-log phase *B. vulgatus* wildtype (WT), *acrR::IN*, and *lpxA::IN* (genome location 362422) strains cultured in the absence of retinol. Transcript counts, normalized by DESeq2, for each gene in the putative *BVU0244-BVU0233* operon are shown. Bars indicate mean ± SEM values for n=3 independent cultures of each strain. Significant differences in gene expression were defined by DESeq2 analysis. *P<0.05; **, P<0.01; ***, P<0.001.

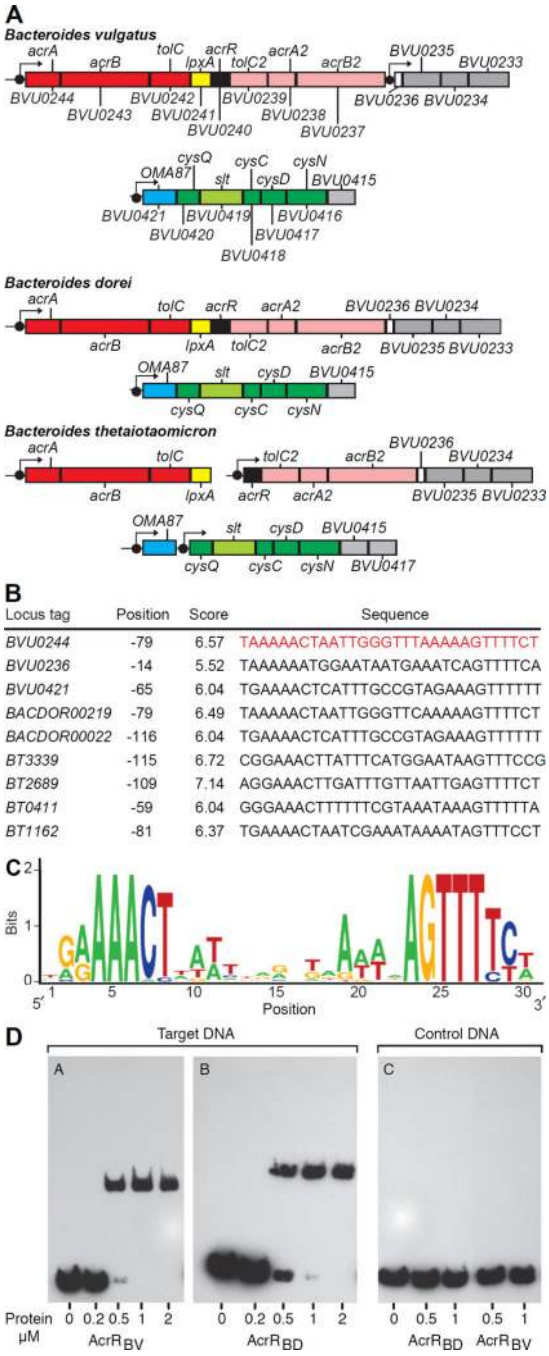

Fig. 5. Interactions between the AcrR transcription factor and its target DNA binding site

(**A**) Predicted AcrR-regulated operons in the genomes of human gut *Bacteroides* species. Boxes indicate clusters of co-regulated genes. Filled black circles indicate predicted AcrR binding sites. Orthologous gene symbols are indicated for each species; unnamed genes are indicated using the orthologous *B. vulgatus* locus designation. (**B**) Sequences of predicted AcrR binding sites. (**C**) Consensus binding site motif. (**D**) Electrophoretic mobility shift assay of the interactions between $AcrR_{BV}$ and $AcrR_{BD}$ and their predicted target DNA sequence.

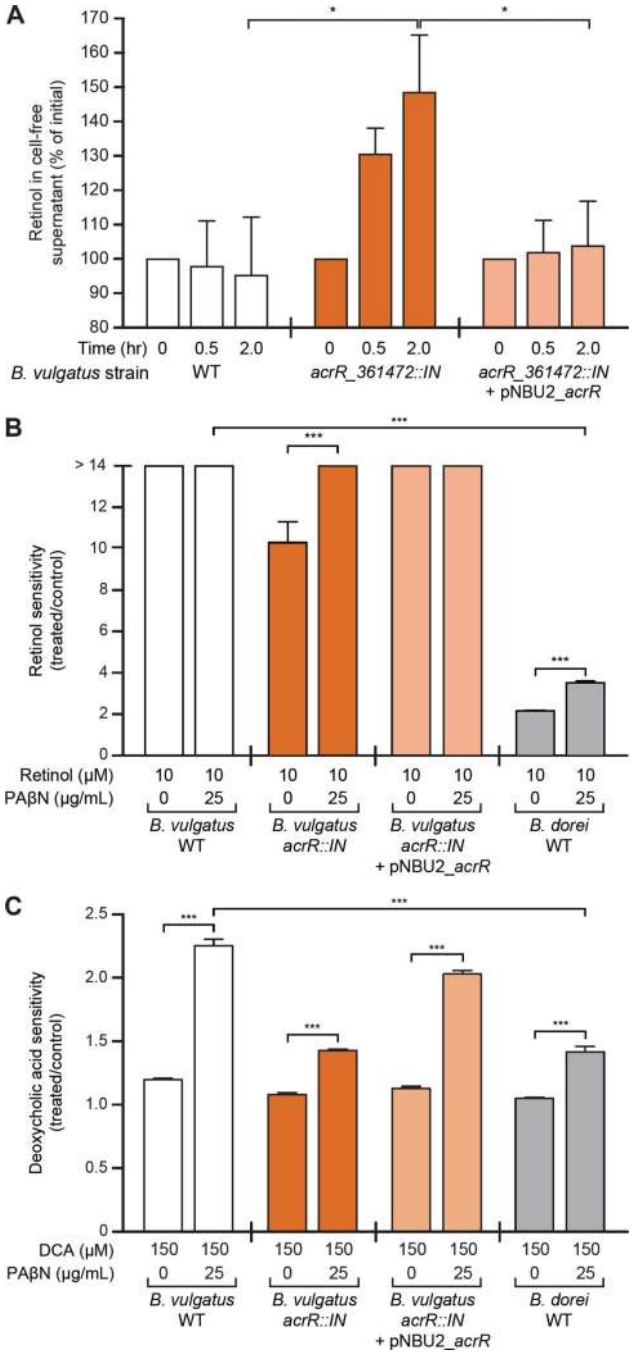

Fig. 6. Role of the AcrAB-TolC efflux pump in regulating the sensitivity of *B. vulgatus* to retinol and deoxycholic acid

(**A**) Retinol efflux assay. Stationary phase cultures of the wildtype (WT), *acrR::IN*, and complemented *acrR::IN* + pNBU2_*acrR* strains were resuspended in PBS containing cysteine and 10 μM retinol. Samples were collected over a 2-h time period and retinol concentrations in cell-free supernatants (CFS) were quantified by UPLC-mass spectrometry. Four independent experiments were performed; n=1–3 replicates per experiment (two-way, repeated measures ANOVA, Tukey's HSD test applied). (**B**) Sensitivity of the wildtype

(WT), *acrR::IN*, and *acrR*-complemented strains of *B. vulgatus*, and wildtype *B. dorei* to 10 μM retinol in the presence and absence of phenylalanine-arginine β-naphthylamide (PAβN), a chemical inhibitor of multidrug efflux systems (see table S15A for further details). Data shown represent one experiment, performed in triplicate (one-way ANOVA, Bonferroni multiple comparisons test). (**C**) The sensitivity of *B. vulgatus* and *B. dorei* strains to deoxycholic acid (DCA) in the presence and absence of PAβN. Data shown represent one experiment, performed in triplicate (one-way ANOVA, Bonferroni multiple comparisons test). Mean values ± SEM are shown. *, $P<0.05$; **, $P<0.01$; ***, $P<0.001$.